Characterization of Lineage-Traced *Sftpc progenitor cells* in the Bronchi (LTS-B) during lung homeostasis and after injury in mice

Inaugural Dissertation
submitted to the
Faculty of Medicine
in partial fulfillment of the requirements
for the PhD degree
of the Faculties of Veterinary Medicine and Medicine
of the Justus Liebig University Giessen

By
Afshin Noori
of
Tehran, Iran

Giessen 2025

From the Department of Internal Medicine II
Director: Prof. Dr. Dr. Friedrich Grimminger
Cardio-Pulmonary Institute (CPI)
Faculty of Medicine of the Justus Liebig University Giessen

First Reviewer and Supervisor: Prof. Dr. Saverio Bellusci
Second Reviewer: Prof. Dr. Nan Tang
Vice Chair and Co-Supervisor: Prof. Dr. Reinhard Dammann
Chair: Prof. Dr. Martin Diener

Date of Doctoral Defense:
26.01.2026

This dissertation is dedicated to my supervisor

Professor Bellusci

for his unconditional Kindness and support

Ehrenwörtliche Erklärung

„Hiermit erkläre ich, dass ich die vorliegende Arbeit selbständig und ohne unzulässige Hilfe oder Benutzung anderer als der angegebenen Hilfsmittel angefertigt habe. Alle Textstellen, die wörtlich oder sinngemäß aus veröffentlichten oder nichtveröffentlichten Schriften entnommen sind, und alle Angaben, die auf mündlichen Auskünften beruhen, sind als solche kenntlich gemacht. Bei den von mir durchgeführten und in der Dissertation erwähnten Untersuchungen habe ich die Grundsätze guter wissenschaftlicher Praxis, wie sie in der „Satzung der Justus-Liebig-Universität Gießen zur Sicherung guter wissenschaftlicher Praxis“ niedergelegt sind, eingehalten sowie ethische, datenschutzrechtliche und tierschutzrechtliche Grundsätze befolgt. Ich versichere, dass Dritte von mir weder unmittelbar noch mittelbar geldwerte Leistungen für Arbeiten erhalten haben, die im Zusammenhang mit dem Inhalt der vorgelegten Dissertation stehen. Die vorgelegte Arbeit wurde weder im Inland noch im Ausland in gleicher oder ähnlicher Form einer anderen Prüfungsbehörde zum Zweck einer Promotion oder eines anderen Prüfungsverfahrens vorgelegt. Alles aus anderen Quellen und von anderen Personen übernommene Material, das in der Arbeit verwendet wurde oder auf welches direkt Bezug genommen wird, wurde als solches kenntlich gemacht. Insbesondere wurden alle Personen genannt, die direkt und indirekt an der Entstehung der vorliegenden Arbeit beteiligt waren. Mit der Überprüfung meiner Arbeit durch eine Plagiatserkennungssoftware bzw. ein internetbasiertes Softwareprogramm erkläre ich mich einverstanden.“

_____

Afshin Noori
Giessen, 2025

Declaration

I declare that I have completed this dissertation single-handedly without the unauthorized help of a second party and only with the assistance acknowledged therein. I have appropriately acknowledged and referenced all text passages that are derived literally from or are based on the content of published or unpublished work of others, and all information that relates to verbal communications. I have abided by the principles of good scientific conduct laid down in the charter of the Justus Liebig University of Giessen in carrying out the investigations described in the dissertation.

_

_____

Afshin Noori

Giessen, 2025

1 Table of Contents

List of figures

Abbreviations and Acronyms

- **ACTA2** – Alpha Smooth Muscle Actin 2 (smooth muscle marker)
- **ADI** – Alveolar Differentiation Intermediate
- **AEP** – Alveolar Epithelial Progenitor
- **AGER** – Advanced Glycosylation End-Product Specific Receptor (RAGE)
- **APC-** – Allophycocyanin-negative (flow cytometry marker)
- **ARDS** – Acute Respiratory Distress Syndrome
- **AT0** – Transitional alveolar progenitor state (between AT2 and AT1)
- **AT1** – Alveolar Type I cell
- **AT2** – Alveolar Type II cell
- **B6 / C57BL/6** – Common inbred laboratory mouse strain
- **BADJ** – Bronchioalveolar Duct Junction
- **BASC** – Bronchioalveolar Stem Cell
- **BMP** – Bone Morphogenetic Protein
- **BSA** – Bovine Serum Albumin
- **CBG** – SPC-BAC-EGFP (*Sftpc* reporter mouse line, “Cecal BAC GFP”)
- **CD200** – Cluster of Differentiation 200 (surface marker)
- **CFE** – Colony Forming Efficiency
- **CHIR / CHIR99021** – Small molecule inhibitor of GSK3, used to activate Wnt signaling
- **CO_2** – Carbon Dioxide
- **COPD** – Chronic Obstructive Pulmonary Disease
- **DMEM** – Dulbecco’s Modified Eagle Medium
- **DNA** – Deoxyribonucleic Acid

- **DTR** – Diphtheria Toxin Receptor
- **EDTA** – Ethylenediaminetetraacetic Acid (chelating agent)
- **EGFP** – Enhanced Green Fluorescent Protein
- **EPCAM** – Epithelial Cell Adhesion Molecule
- **FACS** – Fluorescence-Activated Cell Sorting
- **FASTQ** – File format for storing biological sequencing reads
- **FBS** – Fetal Bovine Serum
- **FGF10** – Fibroblast Growth Factor 10
- **GO** – Gene Ontology
- **H1N1** – Influenza A virus subtype H1N1
- **H2-K1** – Histocompatibility 2, K1 (MHC Class I antigen in mice)
- **IF** – Immunofluorescence
- **IP** – Intraperitoneal (injection)
- **IPF** – Idiopathic Pulmonary Fibrosis
- **KEGG** – Kyoto Encyclopedia of Genes and Genomes
- **KRT17** – Keratin 17
- **KRT5** – Keratin 5
- **KRT8** – Keratin 8
- **KRT18** – Keratin 18
- **LNEP / LNEPS** – Lineage-Negative Epithelial Progenitor(s)
- **LTS-A** – Lineage-Traced *Sftpc*-positive Alveolar cells
- **LTS-B** – Lineage-Traced *Sftpc*-positive Bronchial cells
- **LTS-PCLS** – LTS cells in Precision-Cut Lung Slices
- **LTS-Native** – LTS cells in native lung tissue
- **PBS** – Phosphate-Buffered Saline

- **PBST** – Phosphate-Buffered Saline with Tween
- **PCA** – Principal Component Analysis
- **PCLS** – Precision-Cut Lung Slices
- **PCR** – Polymerase Chain Reaction
- **PFA** – Paraformaldehyde
- **RAS** – Respiratory Airway Secretory cells
- **RBC** – Red Blood Cell
- **RNA** – Ribonucleic Acid
- **SCGB1A1** – Secretoglobin Family 1A Member 1 (club cell marker, CCSP)
- **SCGB3A2** – Secretoglobin Family 3A Member 2
- **SEM** – Standard Error of Mean
- ***SFTPC*** **(SP-C)** – Surfactant Protein C
- **SMA (ACTA2)** – Smooth Muscle Actin
- **SP-B** – Surfactant Protein B
- **SYTOX** – Dead cell stain (nucleic acid stain for viability assays)
- **TRP63** – Tumor Protein P63 (transcription factor, basal cell marker)
- **UMAP** – Uniform Manifold Approximation and Projection
- **UMI** – Unique Molecular Identifier (used in sequencing)
- **WT** – Wild Type
- **YFP** – Yellow Fluorescent Protein

Chapter 1: Introduction

1.1 Overview of Lung Injury and the Importance of Studying It

Increasing trends of lung disease burden attributable to ambient particulate matter, ozone, etc, call for an urgent need to implement specific and effective measures. Lung diseases such as chronic conditions (like COPD) and acute syndromes (such as ARDS) pose a profound global health challenge. COPD alone caused 3.3 million deaths in 2019, with 212 million people affected worldwide (Zou et al., 2022).

More than 3 million people are diagnosed with ARDS each year. The incidence among critically ill patients in intensive care units (ICUs) is 10% and the mortality rate is 40% (Battaglini et al., 2023). Given this dual burden of chronic and acute diseases, studying lung injury is very important for understanding pathophysiological processes and treatment strategies.

1.2 Unique structural features of the respiratory system & regeneration

The lung's three-dimensional architecture consists of intricate interactions between epithelial, mesenchymal, endothelial, and immune cells, which adds complexity to regenerative dynamics. This cellular diversity ensures a balance between stability during homeostasis and plasticity during injury repair. The lung is organized into two major compartments: the airways, which conduct gases, and the alveoli, where gas exchange occurs. It is thought that the lung comprises as many as 40 different cell types (Franks et al., 2008).The epithelium has been the major focus of regenerative studies of the lung to date.

1.3 Conducting airway compartments

The airways that conduct airflow and the distal gas-exchanging alveolar compartment. The most proximal airways, including the trachea and main stem bronchi, contain a pseudostratified structure. These proximal airways are surrounded by cartilaginous rings, which are patterned in a dorsal-ventral manner and a layer of airway smooth muscle cells.

1.3.1 Basal cells

Proximal airways in mice, as well as conducting airways through the terminal bronchioles (TBs) in humans, contain basal cells, which are one of the few validated stem cells in the lung 5–8. Basal cells are defined by the expression of *Trp63* and *cytokeratin 5* (*KRT5*), although heterogeneity within this population is evident as subsets also express markers such as *KRT8*, *Notch2*, or *c-Myb*. Functional studies using lineage tracing with *Krt5*-CreER have established that basal cells are multipotent, able to self-renew and generate ciliated, club, and neuroendocrine cells during homeostasis and after epithelial injury (Rock et al., 2009).

1.3.2 Club cells

Moving distally, the airways are maintained by secretory club cells, which are characterized by their cytoplasm filled with secretory granules and high expression of the secretoglobin *Scgb1a1*. Club cells populate the trachea, bronchi, and bronchioles (Otelea et al., 2023).

1.3.3 Ciliated cells

In the bronchi, ciliated cells, in contrast, play a more specialized role in mucociliary clearance and contribute little to epithelial maintenance under normal or regenerative conditions. Although they do not function as progenitors, under pathological conditions such as chronic inflammation, they may convert into other cell types (Jakwerth et al., 2022; Yaghi & Dolovich, 2016), including goblet cells. This process is associated with airway remodeling in diseases like asthma and chronic obstructive pulmonary disease (Jakwerth et al., 2022).

1.3.4 Pulmonary neuroendocrine cells (PNECs)

Another specialized epithelial cell type, PNECs, can be found individually in the proximal airways or in clusters called neuroepithelial bodies within intralobar regions. In vitro data suggest that these cells respond to chemical or mechanical stimuli by releasing neuropeptides and neurotransmitters, indicating their role as airway sensors (J. Xu et al., 2020).

1.3.5 Bronchioalveolar stem cells (BASCs)

A unique progenitor population known as bronchioalveolar stem cells (BASCs) resides at the bronchioalveolar duct junction (BADJ), the transition zone between bronchioles and alveoli. BASCs co-express Scgb1a1 and *Sftpc*, which are markers for club cells and alveolar type 2 (AT2) cells, respectively. BASCs were first identified based on their proliferation following bleomycin-induced injury, and they were proposed to function as bipotent stem cells capable of giving rise to both airway and alveolar epithelia. Although in vitro assays confirm their multipotency, during homeostasis, their contribution is limited. Lineage tracing suggests that their role in regeneration may be more restricted than originally thought. Notably, BASCs have not yet been identified in human lungs, raising the possibility that they are mouse-specific or that equivalent human populations have yet to be discovered (Liu et al., 2019; Salwig et al., 2019).

1.4 Species Differences in Small Airway Architecture:

Most experimental studies use mice, so it is important to point out both similarities and differences between species. The structure and cell composition of the small airways in larger mammals, including humans, are different from those in mice (Figure 1). In humans, the large airways branch into terminal bronchioles (TBs) and then into respiratory bronchioles (RBs). TBs are surrounded by smooth muscle but do not have cartilage rings. Basal cells are found throughout the airways, including TBs, and appear in smaller numbers in RBs (Weibel et al., 2005).

RBs are a special part of the human lung where alveoli (air sacs) mix with airway passages. The lining of RBs is made up of low, cube-shaped cells. Research has also discovered a unique type of secretory cell in the RBs of humans and ferrets—called respiratory airway secretory cells (RASCs). These cells can renew themselves and make alveolar type II (AT2) cells. The RB region is important because damage here contributes to diseases like COPD, idiopathic pulmonary fibrosis (IPF), and also to lung decline during aging (Basil et al., 2024; Kadur Lakshminarasimha Murthy et al., 2022).

In both humans and mice, the trachea and bronchi contain club cells, multiciliated cells, basal cells, and neuroendocrine cells. But there are key differences: mice do not have basal or goblet cells in their small airways, and their bronchioles connect directly to alveoli without RBs. Instead, mice have a bronchioalveolar duct junction (BADJ) that

contains bronchioalveolar stem cells (BASCs), a cell type not clearly found in humans (H. Xu et al., 2023)

1.5 The gas exchange compartment

Much of what is known about lung alveoli has been shaped by studies of the two major epithelial lineages: alveolar type 1 (AT1) and alveolar type 2 (AT2) cells. The alveolar surface is primarily composed of flattened AT1 cells, which cover more than 90% of the alveolar area and are specialized for efficient gas exchange. In contrast, AT2 cells are cuboidal, more numerous, and carry out two essential functions: secretion of pulmonary surfactant and maintenance of epithelial homeostasis. AT2 cells are strategically positioned at the corners of alveoli, where they make up only ~5% of the alveolar surface area. Despite their limited coverage, they are indispensable as the main progenitor population of the alveoli. Under normal conditions, AT2 cells support epithelial turnover by replenishing both AT1 and AT2 cells. Following injury, they proliferate and differentiate to restore lost AT1 cells, thereby ensuring tissue repair. Lineage-tracing studies have firmly established AT2 cells as the principal stem cell pool of the adult alveolar epithelium (M. J. Evans et al., 1975; Jansing et al., 2017).

Alveolar type 1 (AT1) cells were historically regarded as purely structural elements, forming the epithelial barrier and providing the thin gas-exchange interface with the underlying capillary plexus. They were also long considered terminally differentiated, lacking regenerative capacity or plasticity. However, recent evidence challenges this view, demonstrating that AT1 cells retain significant plasticity. Under conditions of acute injury or disrupted respiratory mechanics, AT1 cells can be reprogrammed to revert into alveolar type 2 (AT2) cells. This conversion is regulated in part by Hippo signaling, which integrates mechanical cues through its role in mechanotransduction (Jain et al., 2015; Negretti et al., 2021).

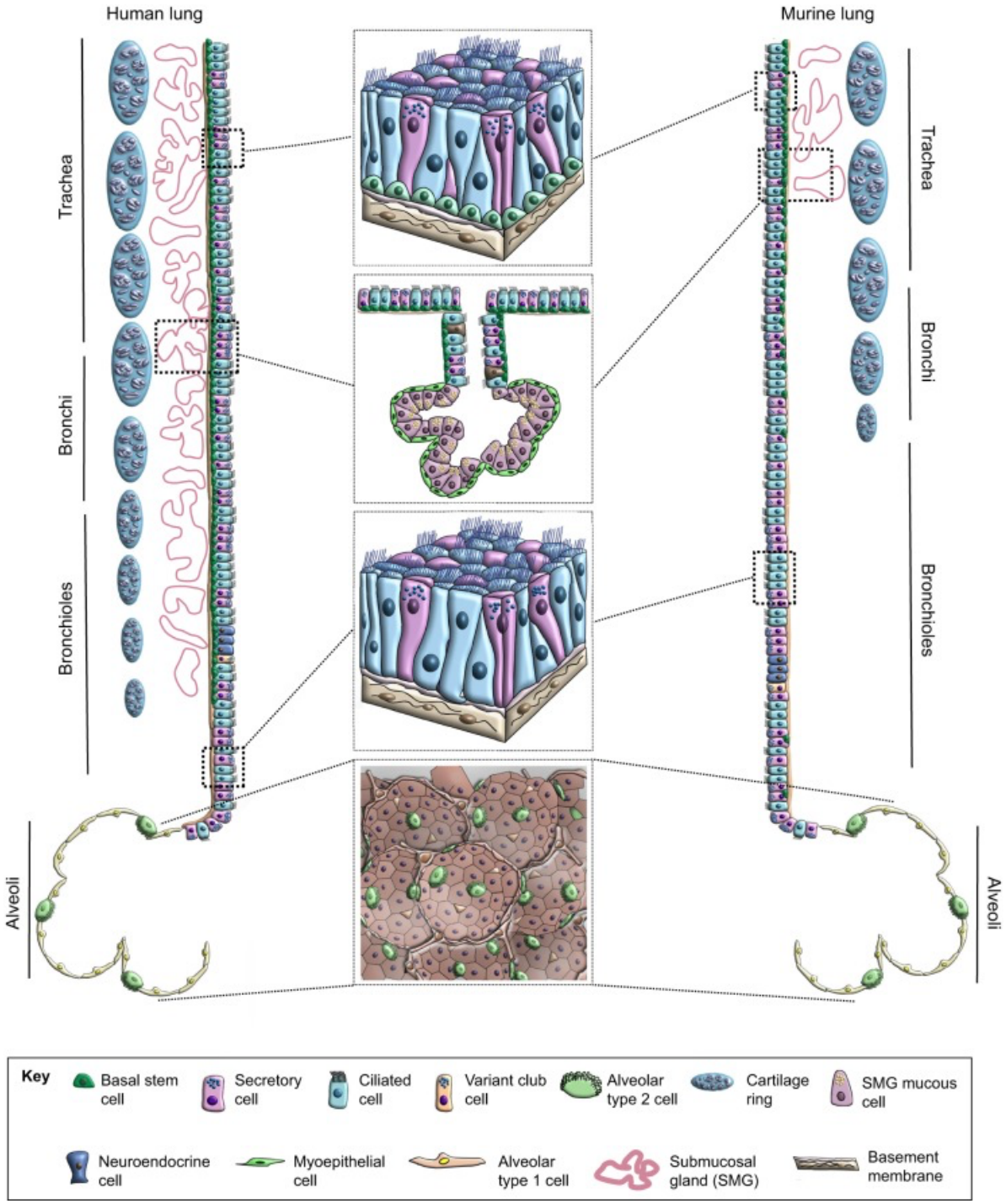

Figure 1: Anatomical and cellular differences between murine and human lung
The respiratory tree is organized into two main regions: the airways and the alveoli. Within the airways, distinct compartments host specialized cell populations that change along the proximodistal axis. In humans, basal cells extend throughout the small airways, whereas in mice, they are confined to the trachea and mainstem bronchi. Cartilage also differs: in humans, rings span several generations of airways, while in mice they are limited to the trachea and mainstem bronchi. Similarly, submucosal glands are widely distributed in human small airways but restricted to the proximal trachea in mice. Other cell types also vary in distribution, as illustrated in schematics. Notably, much of the mouse small airway epithelium is cuboidal, composed mainly of ciliated and secretory cells, whereas in humans this epithelium is confined to the distal bronchioalveolar duct junction picture adopted from (Tata & Rajagopal, 2017).

1.6 *Sftpc*-positive cell heterogeneity

A central molecular feature of AT2 cells is the expression of surfactant protein C (*Sftpc*), which serves as both a functional component of surfactant and a widely accepted lineage marker for this cell type. *Sftpc* is a small hydrophobic protein synthesized as a proprotein (pro-SPC) within the ER, trafficked to lamellar bodies, and secreted into the alveolar lumen as part of the surfactant complex. Within the surfactant monolayer, *Sftpc* plays a role in stabilizing phospholipid films at the air–liquid interface, complementing the actions of surfactant protein B (SP-B). The expression of *Sftpc* is highly specific to AT2 cells, making it an indispensable tool for their identification in both experimental models and human tissue (Mulugeta & Beers, 2006).

For this reason, genetically engineered reporter mouse lines driven by the *Sftpc* promoter (e.g., *Sftpc*-CreER) have become the gold standard for lineage tracing, allowing investigators to follow AT2 cell fate during homeostasis, injury, and repair (Jiang et al., 2020; Lee et al., 2013).

This *Sftpc* positive Cell diversity has been revealed through advances in lineage tracing, single-cell transcriptomics, and functional assays, which demonstrate that subpopulations of AT2 cells differ in proliferation, differentiation, injury response, and stemness potential. Understanding this heterogeneity is central to deciphering how the alveolus maintains homeostasis and regenerates after injury, and it suggests that lung repair is not mediated by a single progenitor pool but rather by multiple, specialized AT2-derived lineages that act in concert or context-dependently (Figure 2) (Chong et al., 2023).

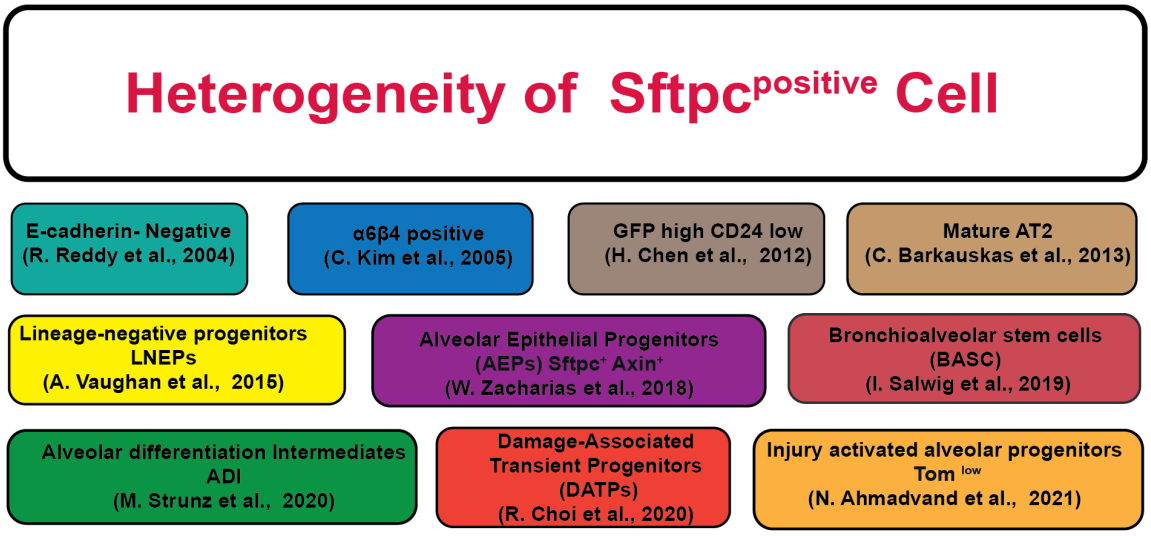

Figure 2 Heterogeneity of different *sftpc*+ cells
Sftpc$^+$ cells comprise diverse progenitor and intermediate subpopulations involved in lung homeostasis and repair. Reported subsets include alveolar differentiation intermediates (ADI, Strunz et al., 2020), GFP^high CD24^low cells (Chen et al., 2012), injury-activated alveolar progenitors (Tom^low, Ahmadvand et al., 2021), damage-associated transient progenitors (DATPs, Choi et al., 2020), and α6β4$^+$ cells (Kim et al., 2005). Additional subsets include E-cadherin–negative cells (Reddy et al., 2004), bronchioalveolar stem cells (BASCs, Salwig et al., 2019), mature AT2 cells (Barkauskas et al., 2013), lineage-negative progenitors (LNEPs, Vaughan et al., 2015), and alveolar epithelial progenitors (AEPs; *Sftpc*$^+$ *Axin2*$^+$, Zacharias et al., 2018). Together, these populations highlight the cellular diversity and regenerative potential within the *Sftpc*$^+$ lineage.

One of the earliest markers used to distinguish AT2 subsets was E-cadherin, which divides rodent AT2 cells into E-cadherin-negative and E-cadherin-positive fractions. These two groups exhibit markedly different responses to hyperoxia-induced stress. E-cadherin-negative AT2 cells show enhanced resistance to oxidative injury, increased proliferation, and higher telomerase activity, while E-cadherin-positive cells are more vulnerable. This dichotomy highlights how differences in adhesion and polarity molecules can underlie functional specialization within the AT2 pool (Reddy et al., 2004).

A second axis of heterogeneity is defined by Wnt responsiveness, marked by Axin2 expression. Axin2-positive AT2 cells represent ~1% of mature *Sftpc*-high AT2 cells in the adult mouse lung, remain stable over time, and demonstrate enhanced clonal expansion and AT1 differentiation in vivo. Their proximity to Pdgfrα+ fibroblasts, which provide Wnt ligands, highlights the importance of niche signals in sustaining their progenitor identity. Building on this, Zacharias et al. identified alveolar epithelial progenitors (AEPs), a conserved Wnt-responsive lineage within the AT2 compartment comprising ~20% of AT2 cells in mice and ~29% in humans. AEPs exhibit a distinct

epigenomic landscape enriched for developmental genes (*Fgfr2, Nkx2.1, Id2, Etv4, Etv5, Foxa1*), and in culture, they display robust organoid-forming capacity that is highly responsive to Wnt and FGF signaling. Their depletion abolishes organoid formation, confirming their identity as a key regenerative subpopulation in both species (Nabhan et al., 2018; Zacharias et al., 2018).

Another distinctive group is defined by integrin α6β4 expression, which marks progenitor-like cells capable of regenerating *Sftpc*+ AT2s following severe epithelial injury. These cells are located at both the bronchioalveolar duct junction (BADJ) and within alveoli, and they exhibit low but detectable levels of *Sftpc* or *Scgb1a1*. Functionally, *α6β4*-positive cells show robust clonal expansion ex vivo, generating heterogeneous colonies that contain both airway and alveolar lineages. Upon injury, they activate *ΔNp63* and *KRT5* programs in a Notch-dependent manner, linking them to repair pathways shared with basal-like cells. By contrast, *α6β4*-negative AT2s, which represent the bulk of the mature population, fail to regenerate clonally, underscoring the rarity and potency of the *α6β4*-positive fraction (Kim et al., 2005).

Additional AT2-derived populations have been identified in the context of injury. Injury-Activated Alveolar Progenitors (IAAPs) represent a distinct subpopulation of AT2-lineage cells that are transcriptionally quiescent under homeostasis but expand significantly after bleomycin injury or pneumonectomy. These cells express low levels of surfactant genes at baseline but activate proliferative and regenerative programs in response to damage. IAAPs contribute to replenishment of the depleted AT2 pool and display plasticity in their ability to self-renew and re-establish alveolar integrity, positioning them as an inducible reserve progenitor population (Ahmadvand et al., 2021; Chong et al., 2023).

Another injury-associated state is represented by Alveolar Differentiation Intermediates (ADIs), transitional cells that arise as AT2s differentiate into AT1s. Identified by single-cell RNA sequencing, ADIs are characterized by *Krt8* expression (Strunz et al., 2020) and overlap significantly with Damage-Associated Transient Progenitors (DATPs), which appear under inflammatory conditions such as IL-1β stimulation. Both populations represent intermediate states along the AT2-to-AT1 trajectory, suggesting that alveolar regeneration proceeds through transcriptionally distinct waypoints rather than direct transdifferentiation. These transitional states may

be particularly relevant in chronic lung disease, where their persistence could impair complete epithelial regeneration (Choi et al., 2020).

AT2 heterogeneity also intersects with populations at the airway alveolar boundaries. Bronchioalveolar stem cells (BASCs), located at the BADJ, co-express Scgb1a1 (club cell marker) and Sftpc (AT2 marker). BASCs exhibit dual lineage potential, capable of regenerating both bronchiolar and alveolar epithelia following injury. While their contribution to alveolar regeneration in vivo remains debated, BASCs provide evidence that AT2 identity can overlap with airway progenitors (Liu et al., 2019; Salwig et al., 2019).

Recently described as a rare Scgb1a1+ progenitor pool lacking mature lineage markers. Lineage-negative progenitors LNEPs proliferate following severe injury and can differentiate into alveolar lineages. Their distinction from BASCs suggests multiple airway progenitor sources contribute to alveolar repair (Vaughan et al., 2015a).

Transgenic mice expressing GFP under the control of the human SFTPC promoter provided a framework to trace airway epithelial heterogeneity during homeostasis and injury. Analysis of GFP signal intensity revealed a spatial organization of epithelial subpopulations: GFP^{low} cells confined to mid-level bronchioles, and GFP^{high} cells distributed within terminal bronchioles and alveoli. Incorporation of Cd24 as a secondary marker distinguished bronchi-associated $GFP^{high}CD24^{low}$ cells from alveolar $GFP^{high}CD24^{high}$ cells, the latter corresponding to type II alveolar epithelial cells (AT2s). Strikingly, in response to bleomycin-induced damage, the bronchi-associated $GFP^{high}CD24^{low}$ subset underwent marked expansion, pointing to their previously unrecognized role as key contributors to epithelial regeneration during lung repair (Chen et al., 2012).

In humans, AT0 cells were recently identified as transitional progenitors at the alveolar–airway interface. These cells co-express AT2, AT1, and secretory markers (e.g., *SFTPC, AGER, SCGB3A2*). Functionally, AT0 cells are bi-potent: capable of differentiating into AT1 or secretory epithelial cells. Their discovery highlights similarities between mouse and human repair paradigms, despite anatomical differences such as the presence of respiratory bronchioles in humans (Kadur Lakshminarasimha Murthy et al., 2022).

1.7 AT2 cells as a stem cell after lung injury

Alveolar type II (AT2) cells function as stem cells in the lung, maintaining the alveolar epithelium by self-renewing and differentiating into alveolar type I (AT1) cells during both normal homeostasis and after injury. Their regenerative capacity and behavior have been extensively studied using various lung injury models, including bleomycin, influenza virus, diphtheria toxin, naphthalene, and precision-cut lung slices (PCLS)(Penkala et al., 2021). These models are essential for investigating different aspects of lung injury and repair, as they aim to replicate the physiological and pathological conditions of the human lung. Each model has its own strengths and limitations, and the choice of model depends on the specific biological processes being studied—such as inflammation, epithelial damage, tissue regeneration, or drug response. Understanding the process of lung regeneration at the cellular and molecular level, including the identification of progenitor cells, is a prerequisite for the development of novel therapeutic strategies

1.7.1 Bleomycin-Induced Injury

Bleomycin is a chemotherapeutic agent that induces DNA damage, leading to injury of multiple alveolar cell types. It triggers transient inflammation and fibrosis, making it a widely used experimental model of idiopathic pulmonary fibrosis (IPF) in mice. During the injury phase of bleomycin-induced lung fibrosis, a significant reduction in the number of AT1 and AT2 cells has been reported
(Barkauskas et al., 2013; Chapman et al., 2011; Rock et al., 2009).
Several studies have been done to identify which progenitor cell populations are activated and contribute to alveolar epithelial repair. One proposed population is bronchioalveolar stem cells (BASCs), which are resistant to both bronchiolar and alveolar injury. Notably, BASC numbers increase approximately 14 days post-bleomycin treatment, suggesting that they may function as alveolar progenitors following the loss of AT1 and AT2 cells. However, it remains unclear whether BASCs differentiate directly into AT1 cells or first become AT2 cells that subsequently convert to AT1 cells (Kim et al., 2005). In a study by Barkauskas et al., the contribution of Scgb1a1^{+} cells to AT2 cell regeneration were investigated using a *Sftpc*CreER; Scgb1a1-CreER; Rosa-Tm triple-heterozygous mouse model. High-dose tamoxifen was administered to induce Cre recombination, thereby labeling AT2 cells (*Sftpc*$^{+}$), double-positive *Sftpc*$^{+}$/*Scgb1a1*$^{+}$ cells located at the bronchioalveolar duct junction

(BADJ), and Scgb1a1$^+$ cells throughout the bronchioles. After intratracheal bleomycin administration, AT2 cell depletion was assessed 21 days post-injury. In comparison to *Sftpc*CreER; Rosa-Tm mice, which showed a marked reduction in labeled AT2 cells, the triple-heterozygous mice exhibited a significantly smaller decrease in AT2 cell numbers. This suggests that Scgb1a1$^+$ cells contribute to the regeneration of AT2 cells. Nevertheless, additional unidentified sources may also play a role in replenishing the AT2 population during repair (Barkauskas et al., 2013; Zheng et al., 2012).

1.7.2 Influenza Virus-Induced Injury

Influenza virus infection induces damage to bronchiolar and alveolar epithelium. After murine-adapted H1N1 (PR8) influenza A infection, the loss of AT1 cells and AT2 cells is evident 5 days post-infection (dpi), which begins to be replaced with newly generated AT2 cells at 11 dpi that are largely increased by 17 dpi and ultimately leads to complete lung recovery after several months (Kumar et al., 2011; Narasaraju et al., 2010)

Different progenitor cells have been introduced as the origin of newly formed AT1 cells and AT2 cells. In a study by Zheng et al., lineage tracing of Scgb1a1- expressing cells showed the appearance of labelled AT2 cells throughout the alveolar region, which compose around 48% of AT2 cells in the damaged parenchyma. Also, labelled AT1 cells were detected among labelled AT2 cells. In the Scgb1a1-CreER lineage tracing system, club cells are the majority of labelled cells, although BASCs and some AT2s are also labelled. In this study, club cells are reported as the source of the majority of regenerated AT2s following severe pulmonary injury induced by influenza virus infection (Zheng et al., 2012). Another key progenitor population contributing to alveolar epithelial repair following influenza-induced injury comprises the Wnt-responsive alveolar epithelial progenitors (AEPs), a specialized subset of AT2 cells traceable using the *Axin2*CreERT2 lineage driver. Zacharias et al. categorized influenza-induced lung injury into four morphologically and functionally distinct zones:

Zone 1: No observable morphological change

Zone 2: Minor injury accompanied by mild interstitial thickening

Zone 3: Pronounced injury with significant alveolar damage

Zone 4: Complete alveolar destruction

One month after influenza infection, AEPs and their lineage-marked progeny remain at homeostatic levels in Zone 1. However, in Zones 2 and 3, where injury severity is

moderate to significant, there's a notable increase in the fraction of lineage-labeled AT2 and AT1 cells, indicating robust proliferation and regenerative activity from the AEP lineage. In contrast, Zone 4 is characterized by the presence of $Krt5^+$ cells, which are not derived from AEPs, underscoring the distinct lineage identity and regenerative limitations of AEPs in severely damaged regions. During the repair process, AEPs exhibit strong self-renewal to maintain their lineage and also produce large numbers of new alveolar epithelial cells. Interestingly, very few non-AEP AT2 cells adopt the AEP phenotype, further reinforcing the lineage autonomy of AEPs (Zacharias et al., 2018).

1.7.3 Hyperoxia-Induced Injury

Prolonged exposure to high oxygen concentrations (>95% O_2) causes oxidative stress and epithelial damage in the lung, especially affecting alveolar and endothelial cells. Studies in mice show that brief hyperoxia between birth and postnatal day 4 causes simplification of the alveoli and a marked loss of type II alveolar (AT2) cells. Because oxygen suppresses proliferation, early exposure is thought to deplete the adult lung of AT2 cells by blocking their initial expansion. Consistent with this, hyperoxia increases expression of AT2 markers (*Sftpc*, *Abca3*) and AT1 markers (*T1α*, *Aquaporin 5*), while reducing the endothelial marker Pecam. BrdU labeling and lineage tracing using *Sftpc* or *Scgb1a1* labeled reporters confirmed that elevated AT2 marker expression at postnatal day 4 reflects transient AT2 cell expansion. However, this population declines upon return to room air, and AT2 cells are nearly absent by eight weeks (Yee et al., 2014). Penkala et al show that AT1 cell plasticity is a mechanism that drives regeneration, beginning in the early postnatal period during alveolar maturation. Upon acute neonatal lung injury, AT1 cells reprogram into AT2 cells, promoting alveolar regeneration. In contrast, the ability of AT2 cells to regenerate AT1 cells is restricted to the mature lung (Penkala et al., 2021). Fibroblast growth factor 10 (Fgf10) is essential for AT2 differentiation in neonatal mice. In Fgf10 heterozygotes ($Fgf10^{+/-}$), the proportion of AT2 cells is reduced compared to wild-type ($Fgf10^{+/+}$) lungs. Remarkably, following hyperoxia exposure, this disparity is no longer apparent by postnatal day 3 (PN3). The normalization in $Fgf10^{+/-}$ mice coincides with elevated cell proliferation after hyperoxic injury, suggesting the activation of compensatory

mechanisms to replenish the AT2 cell pool, although the identity of these restoring cells remains unknown (Chao et al., 2016).

1.7.4 Diphtheria Toxin-Mediated AT2 Depletion

Conditional expression of the human diphtheria toxin receptor (DTR) in alveolar type II (AT2) cells allows selective ablation of this critical progenitor population upon administration of diphtheria toxin. A specialized model of alveolar type II (AT2) cell injury was developed using Sftpc-CreER; Rosa-DTA/Rosa-Tm triple heterozygous mice. Upon tamoxifen administration, AT2 cells expressing Sftpc selectively activate diphtheria toxin A (DTA), leading to targeted AT2 cell apoptosis. Despite widespread AT2 depletion, a resilient subpopulation survives, proliferates, and clonally expands—reestablishing a normal distribution of $Sftpc^+$ AT2 cells by 21 days post-injection (dpi), indicative of complete epithelial repair. Throughout the injury and recovery phases (2, 4, 7, and 21 dpi), lung histology remains remarkably intact, with no evidence of alveolar collapse. High-resolution lineage tracing and imaging confirm that survivor AT2 cells divide clonally, forming discrete clusters, without contribution from $Scgb1a1^+$ club cells located at the bronchoalveolar duct junction (BADJ). These findings illustrate that $Sftpc^+$ AT2 cells act as intrinsic progenitors, capable of self-renewal and regeneration following DTA-mediated injury. Naphthalene-Induced Injury (Barkauskas et al., 2013).

1.7.5 Naphthalene-Induced Injury and Airway/Alveolar Progenitors

Naphthalene is bioactivated by cytochrome P450 enzymes, particularly *Cyp2f2*, into reactive intermediates that selectively ablate club (Clara) cells in the bronchiolar epithelium, leading to epithelial denudation and disruption of the airway lining (Crosby & Waters, 2010) This makes the naphthalene model a widely used platform for probing airway epithelial repair, progenitor cell behavior, and lineage plasticity in response to selective injury (El Agha & Thannickal, 2023).

Following naphthalene injury, a subset of club cells marked by expression of *Scgb1a1* but low or absent *Cyp2f2*, referred to as variant club cells, survive. These cells reside in specialized niches near neuroepithelial bodies (NEBs) and bronchioalveolar duct junctions (BADJs), and function as facultative progenitors, rapidly repopulating the airway epithelium through self-renewal and differentiation into both club and ciliated cells (Kotton & Morrisey, 2014).

With repeated naphthalene exposure, regeneration dynamics become disrupted: some areas exhibit regional hyperproliferation of progenitor cells, while others remain denuded or undergo squamous metaplasia, fueling fibroblast proliferation, peribronchial collagen deposition, and upregulation of fibrogenic cytokines such as TGF-β and CTGF. Chronic club cell depletion ultimately leads to persistent squamous metaplasia and peribronchiolar fibrosis, underscoring the critical role of club cells in airway integrity (Aoshiba et al., 2014).

1.8 Modeling lung physiology and pathology

There are essential platforms for understanding the cellular and molecular mechanisms of damage, repair, and remodeling. Broadly, these models can be divided into in vivo, in vitro, and ex vivo systems.

1.8.1 In Vitro Cell Culture Models

Traditional 2D cell cultures of lung epithelial cells, fibroblasts, or immune cells have been widely used to study specific aspects of lung injury at the cellular and molecular level. These models allow for controlled experiments on isolated cell types, enabling the investigation of cell-specific responses to injury and performing high-throughput screening of drugs.

The differences between human and mouse lungs, along with the strengths and limitations of existing models, highlight the need for complementary human model systems. Yet, maintaining endogenous lung epithelial stem and progenitor cells in vitro remains difficult (Alysandratos et al., 2023). To address this, alternative sources are required for mechanistic studies, disease modeling, drug screening, and the development of cell-based therapies. Approaches using primary cells or pluripotent stem cells (PSCs), including embryonic stem cells (ESCs) and induced pluripotent stem cells (iPSCs), can generate individual lung lineages or complex organoids (Alysandratos et al., 2023; Huang et al., 2015). These in vitro systems not only enable investigation of human lung cell fate and injury responses but also provide a foundation for developing regenerative therapies to restore damaged lung epithelium (Alysandratos et al., 2023).

1.8.1.1 Primary cell or organoid culture systems

3D primary cell culture has enabled ex vivo studies of lung cell organization and fate. Organoid assays using primary or PSC-derived basal and AT2 cells are applied to model development, regeneration, disease, and therapy. Co-cultures combining epithelial and mesenchymal lineages from iPSCs better reflect in vivo biology than single-lineage systems (K. V. Evans & Lee, 2020).

However, primary human AT2 cells are difficult to access and expand, and unlike mouse AT2 cells, they show limited differentiation into AT1 cells. While partial AT2-to-AT1 transitions occur, developmental differences suggest that further refinement of culture systems is needed to fully capture human AT2–AT1 dynamics (Clevers, 2016; Kobayashi et al., 2020).

1.8.1.2 Directed Differentiation of PSCs into Lung Lineages

The in vitro generation of lung epithelium from pluripotent stem cells (PSCs) requires stepwise differentiation that mirrors development, beginning with definitive endoderm and progressing through anterior foregut endoderm. This approach enables the derivation of diverse lung epithelial, mesenchymal, and immune lineages. Key advances came with the identification of signaling pathways—particularly Wnt and BMP—that drive specification of NKX2–1+ primordial lung progenitors. These progenitors, though initially undifferentiated, can give rise to proximal airway cells, basal cells, AT2 cells, and AT1 cells. For example, 3D culture systems have produced iPSC-derived AT2 cells (iAT2s) that closely resemble primary AT2s and secrete surfactant (Huang et al., 2015; Longmire et al., 2012; McCauley et al., 2017; Mou et al., 2012).

Purification of PSC-derived lung progenitors can be improved using genetic reporters (*e.g., NKX2–1, SFTPC, TRP63*) (Gotoh et al., 2014; F. Hawkins et al., 2017; F. J. Hawkins et al., 2021; Jacob et al., 2017). Despite these advances, cultures often contain non-lung endodermal contaminants, and many PSC-derived cells display immature phenotypes. Transcriptomic analyses suggest that differentiation produces a continuum of maturation states, underscoring the need for further optimization before clinical translation (McCauley et al., 2018).

1.8.2 Precision-Cut Lung Slices

Precision-cut lung slices (PCLS) from healthy or diseased human tissue are emerging as a valuable tool to bridge drug discovery and clinical translation. Unlike traditional 2D or 3D organoid systems, PCLS preserve native lung architecture and cellular complexity. They allow parallel testing of multiple treatments in tissue from the same patient, can be prepared from different lung regions, and support ex vivo disease modelling (Alsafadi et al., 2020).

PCLS have provided important insights into disease mechanisms—for example, highlighting Wnt/β-catenin signaling in alveolar repair in COPD (Alsafadi et al., 2020). In IPF, PCLS have been used to investigate therapeutic targets and benchmark the two FDA-approved antifibrotic drugs (Lehmann et al., 2018).

The precision-cut lung slice (PCLS) model is an ex vivo system that preserves both the three-dimensional structure and cellular diversity of lung tissue. Prepared as thin slices (200–400 μm) and maintained in culture for days to weeks, PCLS offer a middle ground between in vitro and in vivo approaches by retaining the native arrangement of epithelial, fibroblast, endothelial, and immune cells, thereby enabling realistic studies of cell–cell interactions. They can be generated from multiple species, including humans, which supports translational research and cross-species comparisons. PCLS also allows dynamic, real-time imaging of cellular processes such as migration, proliferation, and drug responses, while reducing the need for whole-animal studies and aligning with the 3Rs principle (Replacement, Reduction, Refinement) in animal research. However, important limitations remain: the absence of blood and lymphatic circulation alters metabolism and immune responses, tissue viability is generally restricted to short-term culture, and variability in slice preparation can compromise reproducibility and consistency across studies (Koziol-White et al., 2024).

1.8.3 Emerging Models and Technologies

Recent advances in bioengineering have led to the development of additional models, such as organ-on-a-chip technologies and 3D bioprinted lung tissue constructs. These models aim to further mimic the lung's physical and functional characteristics, providing platforms for drug testing and mechanistic studies with enhanced physiological relevance (Barreiro Carpio et al., 2021). Lung-on-a-Chip microfluidic devices recreate the alveolar-capillary interface, with a focus on replicating the mechanical stretching of

the lung during breathing. They allow for the study of cellular responses to mechanical and chemical stimuli in real-time (Zamprogno et al., 2021).

1.8.4 Transgenic Mouse Models

Over the past two decades, transgenic mouse models have been instrumental in advancing our understanding of lung development, homeostasis, and repair. Early strategies relied on lung-specific promoters to constitutively drive transgene expression in defined cell populations. However, these approaches often led to embryonic lethality, limiting their utility in adult studies. The development of conditional transgenic systems overcame this limitation by providing temporal and spatial control of gene expression. These systems have enabled lung-specific gene knockouts, identification of progenitor populations, lineage tracing, and studies of progenitor proliferation and differentiation potential. Among these tools, the Cre-LoxP system remains the most widely used, although alternative recombination strategies are increasingly being applied. Transgenic models are particularly powerful in injury research because they permit precise, cell–type–specific, and temporally controlled genetic manipulation. Their versatility allows interrogation of both baseline functions and dynamic responses to injury. Importantly, combining different genetic systems such as reporter alleles, Cre-loxP recombination, and inducible drivers enables multifaceted analyses of lung biology (Rawlins & Perl, 2012).

1.8.4.1 Reporter Mice Expressing Fluorescent Proteins

Reporter strains in which lineage-specific promoters drive expression of fluorescent proteins (e.g., GFP, YFP, tdTomato) have become essential tools for studying injury biology. These models permit direct visualization of cell populations, real-time monitoring of repair processes, and isolation of live cells for downstream applications such as RNA sequencing or organoid culture. A well-established example is the *Sftpc*-GFP reporter, in which the surfactant protein C (Sftpc) promoter labels alveolar type II (AT2) cells, a key progenitor population in alveolar repair. GFP expression enables selective identification of Sftpc-expressing cells both in situ and during isolation. The SPC-BAC-EGFP (CBG) line was generated by inserting EGFP into the 3′ untranslated region of Sftpc using a bacterial artificial chromosome. In this model, EGFP expression

is confined to pro–SP-C–positive AT2 cells, with uniform fluorescence across all lung lobes that remains stable with age (Vanderbilt et al., 2015).

1.8.4.2 Cre-loxP Driver Lines

Cre-loxP recombination technology, originally developed in the 1980s and first applied to mice in 1998, remains the cornerstone of conditional genetic manipulation in vivo. A mammalian codon-optimized version of Cre recombinase increased efficiency in mammalian systems. The system relies on Cre recombinase, derived from bacteriophage P1, to catalyze recombination between LoxP sites, resulting in excision, inversion, or translocation of the intervening DNA sequence (Sauer & Henderson, 1988). While promoter-driven reporters provide continuous labeling, Cre-loxP driver lines introduce conditionality, enabling permanent lineage tracing or functional manipulation of specific cell populations. For example, *Sftpc*-CreER is widely used to target AT2 cells. Here, Cre is fused to a modified estrogen receptor (CreER), which remains cytoplasmic until tamoxifen administration. Tamoxifen thus provides temporal control, allowing recombination to be induced at specific stages (e.g., before or after injury) (Chapman et al., 2011; Rock et al., 2009).

Applications of Cre-loxP strategies include:

Lineage tracing, when crossed with conditional reporter alleles such as Rosa26-loxP-STOP-loxP-tdTomato (Madisen et al., 2010).

Conditional ablation, when combined with diphtheria toxin receptor alleles, enables selective depletion of defined populations to study their role in regeneration (Nabhan et al., 2018).

1.8.4.3 Crosstalk Between Systems

The most powerful applications of transgenic models arise when reporter strains and Cre drivers are combined (Vanderbilt et al., 2015). For instance, crossing *Sftpc*-CreER mice with Rosa26-tdTomato enables permanent labeling of AT2 cells and their progeny, while *Sftpc*-GFP provides continuous visualization of the same population in live tissues. These complementary tools allow simultaneous lineage tracing, functional manipulation, and real-time monitoring of cellular dynamics during lung injury and repair. This integrated approach now represents a cornerstone of modern lung biology research.

Chapter 2: Objectives

The primary objective of this study was to investigate epithelial progenitor cell dynamics using genetic lineage tracing and fluorescent reporter systems, with a particular focus on identifying novel progenitor populations contributing to alveolar repair. Specifically, we aimed to:

1) Define precision-cut lung slices (PCLS) as a model of acute epithelial injury, with emphasis on the selective vulnerability of alveolar type II (AT2) cells.

2) Characterize the emergence of a novel epithelial progenitor population in the bronchi, termed Lineage-Traced *Sftpc* cells in the Bronchi (LTS-B), identified in *Sftpc*CreERT2; Rosa26-tdTomato; *Sftpc*-GFP mice as tdTomato^{+}/GFP^{-} cells.

3) Determine the behavior of LTS-B cells under different contexts:

In vitro, during PCLS culture, these cells persist in the bronchiolar region and display motility and proliferative capacity.

In vivo, during naphthalene-induced injury, the LTS-B population expands within bronchioles.

4) Assess the plasticity of LTS-B cells, specifically their ability to acquire partial *Sftpc* expression in response to regenerative growth factor treatment (FGF10 and CHIR99021).

5) Explore the potential existence of LTS-B–like populations in bleomycin-injured mouse lungs and in the human idiopathic pulmonary fibrosis (IPF) dataset.

Chapter 3: Material and Methods

3.1 Animal experiments

All animals were housed under specific pathogen-free (SPF) conditions with free access to food and water. Genetically modified mice included Sftpctm1(CreERT2,rtTA)Hap (kind gift from Hal Chapman), the Cre-reporter line tdTomatoflox (B6;129S6-Gt(ROSA)26Sortm9(AG-tdTomato)Hze/J, Jacksonlab strain 007909), the *Sftpc* reporter line (B6N.Cg-Tg(Sftpc,-EGFP)1Dobb/J, Jackson lab strain 028356). All animal husbandry and the following experiments were approved by the Institutional Animal Care and Use Committees at JLU, following German National guidelines. A tamoxifen stock solution was prepared by dissolving tamoxifen powder (Sigma Aldrich; T5648-5G) in corn oil at a concentration of 20 mg/mL at room temperature and stored at −20 °C. Female and male *Sftpc*CreERT2; tdTomatoflox mice aged 8 to 24 weeks received intraperitoneal injections of tamoxifen (0.1 mL/10 g of body weight) on alternate days for a total of three injections (G7/2017–No.844-GP and JLU-775).

The following experiments were approved by the Institutional Animal Care and Use Committees at the Oujiang lab (OJLAB24091813). Female and male *Sftpc*CreERT2; tdTomatoflox *Sftpc*GFP mice aged 8 to 24 weeks received intraperitoneal injections of tamoxifen (0.1 mL/10 g of body weight) on alternate days for a total of three injections. Naphthalene injury on *Sftpc*CreERT2; tdTomatoflox mice was carried out. Naphthalene was dissolved in corn oil at a concentration of 20 mg/mL at room temperature and stored at −20 °C. Only female mice aged 8 to 24 weeks received intraperitoneal injections of Naphthalene (0.1 mL/10 g of body weight) once, 5 days before sacrifice. Mice were maintained on a C57BL/6 background. Both sexes were used for this study.

3.2 Mice Genotyping

Mice ear mark biopsies were digested in 200 µl Viagen, including 2 µl proteinase K at 55°C on a thermomixer comfort overnight, and then the reaction was stopped at 85°C for 40 min. Next, PCR was employed to amplify DNA using specific primers (Table 1). The PCR product of the samples was then analyzed using a QIAxcel capillary gel electrophoresis instrument (Qiagen, 9002123).

Table 1: Protocols for genotyping and band size of PCR product						
Mouse line	Expected band size		Primer sequences	PCR protocol		
	WT	Mutant		step	Temp. (°C)	Time
SftpcCreERT2	500 bp	1000 bp	1) CCC AGT CCC TCT CTG AAT TTG 2) GTT TCT ACC GAC CCT GTG AAG 3) CAT CGC TCG ACC AGT TTA GTT A	1	95	3 min
				2	95	30 sec
				3	50	30 sec
				4	72	1:15 min repeat 2-4 (35 cycles total)
				5	72	5 min
				6	4	hold
tdTomatoflox	850 bp	297 bp	1) CTG TTC CTG TAC GGC ATG G 2) GGC ATT AAA GCA GCG TAT CC 3) CCG AAA ATC TGT GGG AAG TC 4) AAG GGA GCT GCA GTG GAG TA	1	94	3 min
				2	94	20 sec
				3	61	30 sec
				4	72	1:30 min repeat 2-4 (40 cycles total)
				5	72	2 min
				6	4	hold
CBG	324bp	340bp	1) GTA GGT GGA AAT TCT AGC ATC ATC C 2) ACC CTG TGT GGA GAG CTA CC 3) CTA GGC CAC AGA ATT GAA AGA TCT 4) GTA GGT GGA AAT TCT AGC ATC ATC C	1	94	3 min
				2	94	20 sec
				3	65	30 sec
				4	68	1 min repeat 2-4 (10 cycle total)
				5	94	15 sec
				6	60	15 sec
				7	72	10 sec repeat 5-7 (28 cycle total)
				8	72	1 min
				9	4	hold

3.3 Human specimens

Human lung tissues from the donor. Patients undergoing lung transplantation were provided with donors from the Giessen biobank. The study protocol was approved by the ethics committee of the University of Giessen, which conforms to the principles outlined in the Declaration of Helsinki. Tissues were subjected to RNA extraction and gene expression analysis by qPCR.

3.4 Precision Cut Lung slices

Precision-cut lung slices from the mouse lung were prepared under sterile conditions. Lungs were flushed via the heart with sterile phosphate-buffered saline (PBS). A shielded I.V. catheter (Braunüle Vasofix, 4268113S-01) was carefully inserted through the trachea under the jaw above the bifurcation of the principal bronchi and fixed in place by clamps. After cannulation and dissection of the diaphragm, lungs were slowly injected with 1.7% low-melting-point agarose (Sigma Aldrich, A9414) in PBS to fully inflate both lungs until the tip of the accessory lobe was inflated. The trachea was then

ligated with thread to retain the agarose inside the lungs. Afterward, the lungs were excised and transferred to a tube with PBS and cooled on ice for 10 min to allow the agarose to solidify. Each lung lobe was separated and cut with a vibratome (LEICA VT1200) to a thickness of 300 µm (1 mm/s speed, 85 Hz frequency, 1.5 mm amplitude). PCLS were obtained from all lobes and placed immediately in a 6-well plate with approximately 2 mL of culture medium (DMEM: Glutamax (Gibco, 21885025), supplemented with 1% penicillin/streptomycin (Gibco, 15140122), 100 µg/ml of Normocin (Invivogen, ant-nr-05), and 10 % fetal bovine serum (Gibco, A5256801) per well at 37°C (8-10 PCLS/well). The overall process from sacrificing the mice to the generation of PCLS is done within 1 hour to minimize epithelial damage. Slices were kept fully submerged and cultured at 37°C, 5% in humidified conditions. Medium was changed every other day.

3.5 Live imaging of PCLS

For imaging, PCLS were positioned flat inside a special insert for 6-well plates (0.4 µm PET translucent, Item number: 9300402, CellQART). The insert was then transferred to a well containing exactly 2 mL of culture medium. Our imaging system combines a standard inverted fluorescent microscope (Leica-Microsystems, DMI-6000) with an incubation chamber to control humidity, temperature, and CO_2. To ensure and maintain optimal culture conditions, each PCLS was submerged in culture medium. PCLS were then left in the incubator for 8 days. Time-lapse fluorescence imaging at 1 frame/4 hours for up to 185 hours per PCLS. Corresponding bright-field pictures to identify the alveolar and bronchiolar regions were acquired. The tdTomato positive area and corresponding mean intensity in bronchial and alveolar regions were quantified over time with the use of ImageJ/Fiji (Schindelin et al., 2012).

3.6 Confocal Live imaging of PCLS

For confocal imaging, PCLS were positioned, fixed, and flat on the glass bottom of a chambered coverslip (Ibidi 80421) and imaged on an inverted confocal microscope (Leica-Microsystems, SP8) equipped with an incubation chamber to control humidity, temperature, and CO_2. PCLSs were imaged for up to 4 days. Multiple tile-scans per PCLS were acquired every two hours with a 10x0.4NA objective for up to 96 hours, using LAS-X software (version 3.5.7). For every acquisition, we excited the tdTomato

and the eGFP fluorophores using the 553nm and 499nm laser lines, respectively, derived from a White Light Laser. Additionally, we captured the transmitted 553nm light to identify alveolar and bronchiolar regions. Upon registration of the resulted time-lapses, the data were opened with Imaris to investigate the expression levels of tdTomato and eGFP over time.

3.7 Immunofluorescence and Fluorescence quantification

PCLS were fixed with 4% paraformaldehyde (PFA, Roth, P087.3) and washed in PBS. Antigen retrieval was performed in citrate buffer, pH 6.0 (Sigma-Aldrich, P4809) using a water bath (95°C for 3-5 min in a rice cooker). Sections were washed with 0.4% Triton X-100 in PBS (PBST), incubated in blocking buffer (3% BSA in 0.1% PBST) for 1 h, and then stained overnight with primary antibody at 4°C. Following primary antibody incubation, tissues were washed three times in PBST, followed by incubation with secondary antibody in blocking buffer for 2 h. Sections were washed with PBST. Primary antibodies used were: Acta2 Conjugated (Millipore, ab3786, 1:500), Scgb1a1 (R&D systems, MAB1179, 1:500), TdTomato (Origene, AB8181-200, 1:700), Krt8 (Sigma, HPA030180-100UL, 1:500), Krt18 (Vector laboratories, DL-1178, 1:1000). Images were captured on an Olympus FV3000 confocal microscope at 20X magnification.

3.8 Flow cytometry

Adult mice were sacrificed, and lungs were perfused with 5 mL PBS through the right ventricle. Lungs were inflated via the trachea with dispase and kept in dispase (Stemcell, 07913) and collagenase Type I (Gibco, 17018029) at 37°C for 40 min with frequent agitation. To achieve single cell suspensions, digested tissue was passed serially through 100-, 70-, and 40-µm cell strainers (Greiner Bio-One, 542000). Red blood cells (RBC) were eliminated using RBC lysis buffer (Sigma-Aldrich, 11814389001) according to the manufacturer's protocol. Cells were pelleted, resuspended in FACS buffer (0.1% sodium azide, 5% fetal bovine serum (FBS, Gibco, A5256801), 0,05% EDTA in PBS), and stained with antibodies: anti-Epcam (APC-Cy7-conjugated, Biolegend,1:50, 118218), anti-Cd45 (BV711-conjugated, Biolegend, 1:50, 103147), and anti-Cd31 (BV711-conjugated, Biolegend, 1:50, 102449) antibodies for 20 min on ice in the dark, followed by washing. Next, cells were washed and stained

with SYTOX (Invitrogen, S11348), a live/dead cell stain, according to the manufacturer's instructions. Flow cytometry data acquisition and cell sorting were carried out using the BD FACSymphony cell sorter (BD Biosciences, San Jose/CA). Data were analyzed in FlowJo v10 (FlowJo, LLC).

3.9 RNA extraction

Sorted cells were homogenized using a Qiagen TissueLyser II with 5-mm stainless steel beads in TRIzol at 27 Hz for 3 to 5 min. TRIzol homogenates were mixed with chloroform (5:1, vol/vol) and incubated for 15 min, followed by centrifugation (12,000 g) for 15 min at 4°C. The aqueous phase was then mixed with an equal part of 70% ethanol. RNA purification was performed according to the manufacturer's instructions with the MagMAX™-96 Total RNA Isolation Kit (Invitrogen, AM1830). Samples were stored at −80°C until further analysis. RNA concentration was measured using Nanodrop [spectrometry; absorbance at 260 nm (A260)], and Qubit RNA HS Assay Kit (Invitrogen; fluorescence).

3.10 Bulk RNA-seq

For genome-wide analysis of gene expression, RNA sequencing libraries from polyadenylated mRNA were generated and sequenced by the Institute for Lung Health (ILH) – Genomics and Bioinformatics – at the Justus-Liebig-University (JLU) Giessen (Germany). Total RNA was used for cDNA sequencing library preparation utilizing the NEBNext® Single Cell/Low Input RNA Library Prep Kit for Illumina® (New England BioLabs) according to the manufacturer's instructions. After library quality control by capillary electrophoresis (4200 TapeStation, Agilent), cDNA libraries were sequenced on the Illumina NovaSeq 6000 platform, generating 50 bp paired-end reads. The Illumina software bcl2fastq (v2.20.0.422) was utilized for demultiplexing and generating FASTQ files. Initial processing of the sequencing reads—comprising quality control, filtering, trimming, alignment, and the creation of gene-specific count tables-was conducted using the nf-core RNA-seq v3.7 bioinformatics pipeline, with the Mus musculus mm10 and gene annotations sourced from Illumina's iGenome repository. The pipeline ran with default parameter settings in Docker mode. Subsequent analysis, including raw read count normalization and differential gene expression detection, was performed in R using DESeq2. Raw sequencing data and derived gene expression

matrix have been uploaded to NCBI's Gene Expression Omnibus under accession number GSE (pending). Excel files corresponding to the differentially expressed genes for the different comparisons are submitted in the supplementary data section.

3.11 Alveolosphere assay

Sorted epithelial cells positive for both tomato and GFP (LTS-A) as well as cells positive for tomato and negative for GFP (LTS-B), were isolated from the lungs of *Sftpc*CreERT2/+; tdTomflox/flox; *Sftpc*GFP mice previously treated with tamoxifen. Resident mesenchymal cells from wild type C57BL/6J mice (Epcam-, Cd31-, Cd45-, Sca1+) were also isolated. The cells were centrifuged and resuspended separately in cell culture medium (Dulbecco's Modified Eagle Medium, Life Technologies). 1x103 epithelial cells in 25 µL media and 2x104 mesenchymal cells in 25 µL media per insert (12 mm cell culture inserts with 0.4 µm membrane, Millipore) were used. Mesenchymal and epithelial cell suspensions were mixed, followed by the addition of cold Matrigel® growth factor-reduced (Corning, CLS356230-1EA) at a 1:1 dilution, resulting in a 100 µL final volume per insert. Matrigel cell suspensions were placed on the top of the filter membrane of the insert and incubated at 37°C for 5 min. Next, 350 µL of the medium was transferred to each well. Cells were incubated under air-liquid conditions at 37°C with 5% CO_2 for two weeks. Media were changed 3 times per week.

3.12 Generation of the scRNA-seq data:

Live sorted tdTom+ cells were centrifuged and resuspended in 0.04% ultrapure BSA (Invitrogen, 01266574) in PBS for optimal cell concentration. The resuspended tdTom+ cells were loaded into the Chromium Controller (10x Genomics), and the cDNA libraries were prepared according to the manufacturer's instructions. scRNA-Seq libraries were sequenced on the Illumina NovaSeq 6000 or NextSeq 2000 platform with the following sequencing settings: Read 1: 28 bp, Read 2: 90 bp, Index 1: 10 bp, Index 2: 10 bp, and reads were aligned against a custom mouse reference genome (mm10) and counted by STARsolo.

3.13 Analysis of the scRNA-seq data:

All downstream analyses were carried out with the Seurat R package (v4.1.0) (Hao et al., 2024). First, the count matrix of each sequenced sample was loaded as a Seurat

object, then filtered using arbitrary thresholds for UMI, genes, and mitochondrial content (nCount_RNA < 30000, nFeature_RNA > 800, and percent. mito < 0.25), before being concatenated. The concatenated matrix was normalized using the NormalizeData function. After normalization, the counts of the 2000 most variable features selected with the “vst” method were scaled and centered before running PCA. Harmony (Korsunsky et al., 2019) was run on the PCA cell embedding, specifying the sample of origin as a covariate. kNN clustering was run on the first 50 dimensions computed with Harmony (using k. param =10), same for UMAP visualizations in two dimensions. Based on UMI content and differentially expressed genes in each cluster, clusters corresponding either to remaining low-quality cells or non-mesenchymal cells were removed. The integration process was run again on the subset of selected cells with the same parameters. Finally, cell clusters were annotated according to the expression of their specific markers. Differential expression between samples for a particular subpopulation was run using the FindMarkers function on normalized data. Gene overlap and pathway analysis were conducted with Metascape (metascape.org) by interrogating GeneOntology, WikiPathways, and Reactome databases. Human integration was performed within a standard Seurat workflow (Jurado et al., 2024). First, the Import function was used to generate Seurat objects from the scRNA-seq data. Second, orthologous genes were identified using the BuildOrtholog function. Finally, the IntegrateObjects function was applied to create an integrated object with a uniform gene nomenclature across species

3.14 Cell death and proliferation assays (EdU)

Labelling of proliferative cells was carried out using 5-ethynyl-2-deoxyuridine (EdU) in culture medium as recommended by the manufacturer. After incorporation of EdU, the target tissue was fixed in formalin and stained according to the manufacturer's instructions. With CellEvent Caspase-3/7, detect activated caspase-3/7 in live cells in pcls to detect fluorogenic substrates for apoptosis (Invitrogen, C10423). The LIVE/DEAD™ Fixable Far-Red Dead Cell Stain Kit (Invitrogen, L10120) was used to determine the viability of cells before the fixation. Permeabilization is required for intracellular antibody staining or before the elimination of biohazardous materials using formaldehyde fixation.

3.15 Statistical analysis

Statistical analysis and graph assembly were carried out using GraphPad Prism 6 (GraphPad Prism Software). Significance was determined by unpaired two-tailed Student's t-tests. Data are presented as mean ± standard error of mean (SEM). Values of $p < 0.05$ were considered significant. The number of biological samples (n) for each group is stated in the corresponding figure legends.

Chapter 4: Results

In this chapter, we first establish PCLS culture as a reproducible ex vivo injury model (Section 4.1). Then, we identify a rare Sftpc-lineage population localized to the bronchi (LTS-B) and define its baseline phenotype and heterogeneity (Sections 4.2–4.3). Next, we test the injury responsiveness of LTS-B in vivo (naphthalene) and in vitro (PCLS) and determine whether injury drives a transitional ADI-like state (Sections 4.4–4.5). Lastly, we examine if pro-regenerative cues (FGF10+CHIR) can promote AT2 commitment of LTS-derived transitional cells. We validate this trajectory using live confocal imaging and scRNA-seq while distinguishing LTS-B from BASCs (Sections 4.6–4.8).

4.1 Define PCLS as a model of acute epithelial injury, with emphasis on the selective vulnerability of alveolar type II (AT2) cells.

Both human and mouse precision-cut lung slices (PCLS) displayed an early injury response, as reflected by the rapid decline of epithelial and signaling markers, such as *SFTPC, EPCAM, SCGB1A1, FGFR2B,* and *FGF10*, shortly after culture. This loss indicates acute epithelial stress and disruption of homeostatic signaling pathways. After the initial drop, however, both FGF10 and the mesenchymal marker *ACTA2* showed signs of recovery in PCLS from both species over time, suggesting the initiation of a regenerative response. The re-emergence of FGF10, a key developmental growth factor, together with ACTA2, a marker of activated fibroblasts and tissue remodeling, highlights PCLS's capacity to initiate a partial repair program despite culture-induced injury (Figure 3).

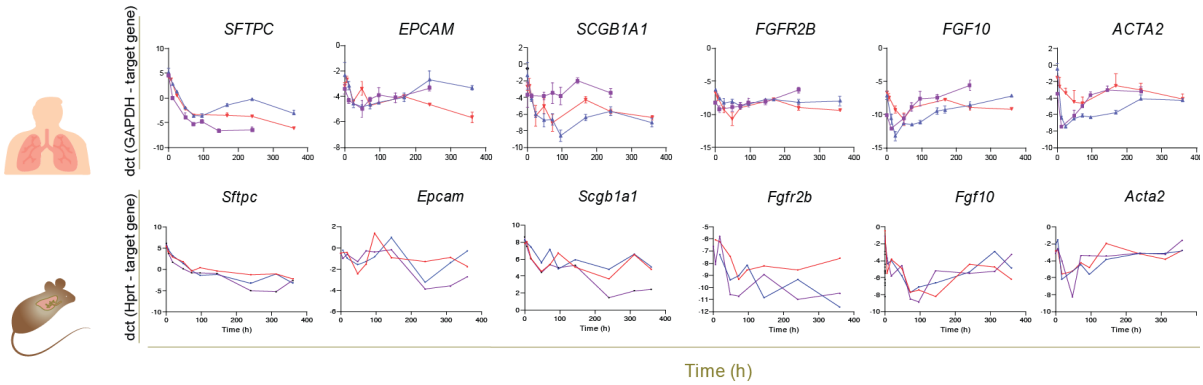

Figure 3: **epithelial cell damage and ongoing repair by qPCR**
qPCR analysis of key epithelial (*SFTPC/Sftpc*, *EPCAM/Epcam*, *SCGB1A1/Scgb1a1*) and mesenchymal (*FGFR2B/Fgfr2b*, *FGF10/Fgf10, ACTA2/Acta2*) markers over time in human (top, normalized to *GAPDH*) and mouse (bottom, normalized to *Hprt*) lung tissues. Expression changes are shown as ΔCt values across indicated time points (h), illustrating conserved and divergent temporal regulation between species.

In summary, PCLS culture induces a rapid and consistent epithelial injury program in both mouse and human tissue slices. This is followed by the partial reactivation of mesenchymal/regenerative signaling (FGF10) and a remodeling response (ACTA2). These processes create a controlled ex vivo environment in which the behaviors of epithelial progenitors can be tracked during a defined injury-repair period (Figure 3).

4.2 Characterization of Lineage-Traced *Sftpc* progenitor cells in the Bronchi (LTS-B)

Characterization of lineage-traced *Sftpc*-positive cells during homeostasis revealed the presence of a discrete population of tdTom-positive, negative for *Sftpc*GFP in the bronchial epithelium. We used tamoxifen administration in vivo in *Sftpc*CreERT2 mice combined with Tomatoflox and *Sftpc*GFP mice (Figure 5A) and characterized the different lineage-labeled epithelial populations by IF and FACS on lung sections, tdTom+*Sftpc*GFP+ cells (yellow in Figure 5B) were present in alveoli and correspond mostly to alveolar type 2 cells (AT2); we refer to these as LTS-A cells. We also identified tdTom+ cells that were negative for *Sftpc*GFP (red) in the bronchi; we refer to these as LTS-B cells (Figure 4 shows LTS-B cells along the proximal-distal axis of the bronchi in *Sftpc*CreERT2; tdTomatoflox mice). tdTomatoflox mice negative for *Sftpc*CreERT2 treated with or without tamoxifen did not display tdTom+ cells, indicating that our transgenic tool relies on *Sftpc*CreERT2 for cell labeling.

Next, we characterized these different subpopulations by FACS (Figure 5C). After exclusion of endothelial and hematopoietic cells using Cd31 and Cd45 antibodies,

respectively, the epithelial subpopulation was isolated using Epcam antibodies. Epcam+Cd31-Cd45- epithelial cells were further investigated for tdTom and GFP expression. Our FACS plot in Figure 5C indicates the presence of two major populations. An overwhelming majority (90.5%) expressed both tdTom and *Sftpc*GFP and corresponded to LTS-A cells (mature AT2s). However, a small fraction (1.6%) expressed tdTom but were negative for *Sftpc*GFP. These cells correspond to LTS-B cells. LTS-B cells are not labeled with Lysotracker (Figure 5C), which stains specifically the lamellar body characteristic of mature AT2 cells. In addition, further analysis indicated that LTS-B are negative for *Sftpc* expression by IF (data not shown). These results support that LTS-B cells are different from mature AT2s, even though they are lineage-traced using the *Sftpc*CreERT2 driver line. Please note that only a very small fraction (0.23%) of Epcam+Cd31-Cd45- cells were negative for tdTom but positive for *Sftpc*GFP, indicating that in our experimental conditions, the labeling of AT2s after tamoxifen administration is very efficient as previously reported (Ahmadvand et al., 2021). Figure 5D summarizes in a schematic the localization of LTS-A and LTS-B cells in the alveoli and bronchi, respectively.

Next, we tested the capacity of LTS-A and LTS-B cells to form organoids in vitro when recombined with lung mesenchymal niche cells (Cd31-Cd45-Epcam-Sca1+ cells as previously described (Taghizadeh et al., 2021). LTS-B cells failed to form alveolospheres, indicating their quiescent nature (Figure 5E), while the CFE and size of the alveolospheres generated with LTS-A cells were as previously reported with mature AT2s (Figure 5F) (Ahmadvand et al., 2021; Taghizadeh et al., 2021).

Next, we carried out bulk RNA-seq on LTS-A and LTS-B cells. Signature score analysis indicates that LTS-B cells displayed a decrease in the AT2 and ADI (intermediate AT2/AT1 cells) signature compared to LTS-A cells. By contrast, LTS-B cells displayed increased Club and Ciliated cell signatures compared to LTS-A (Figure 5G). Upregulated genes in KEGG between LTS-B and LTS-A cells (Figure 5H) and the enrichment score analysis (Figure 5I) identified the differential activation of the PI3k-Akt signaling pathway in LTS-B, as well as a lower level of Fgf signaling (Figure 5I). Finally, the volcano plot in Figure 5J indicated the enrichment of *Igfbp5, Scgb1a1*, and *Scgb3a2*, the latter being a marker of a progenitor cell population previously described in the terminal bronchioles in humans (Kadur Lakshminarasimha Murthy et al., 2022).

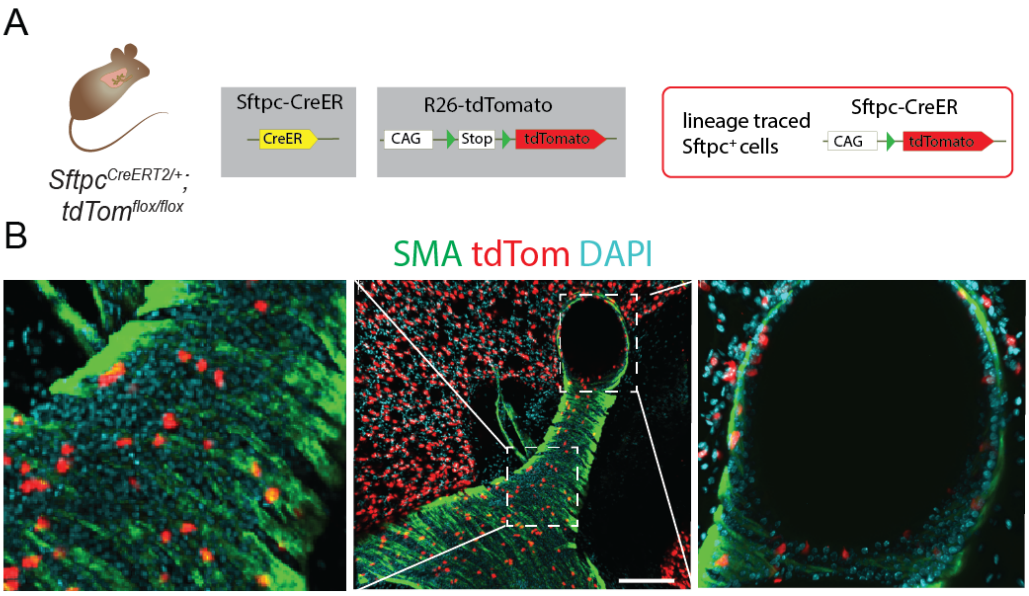

Figure 4: LTS location in bronchi in homeostasis.
A) *Sftpc*CreERT2 mice combined with Tomatoflox. B) *Sftpc*CreERT2 positive cells are spread out along the proximal-distal axis of the bronchi (middle picture). High magnification of the bronchi is shown in the left picture. The right picture shows that these lineage-labeled cells are found in the apical side of the bronchial smooth muscle cells expressing SMA

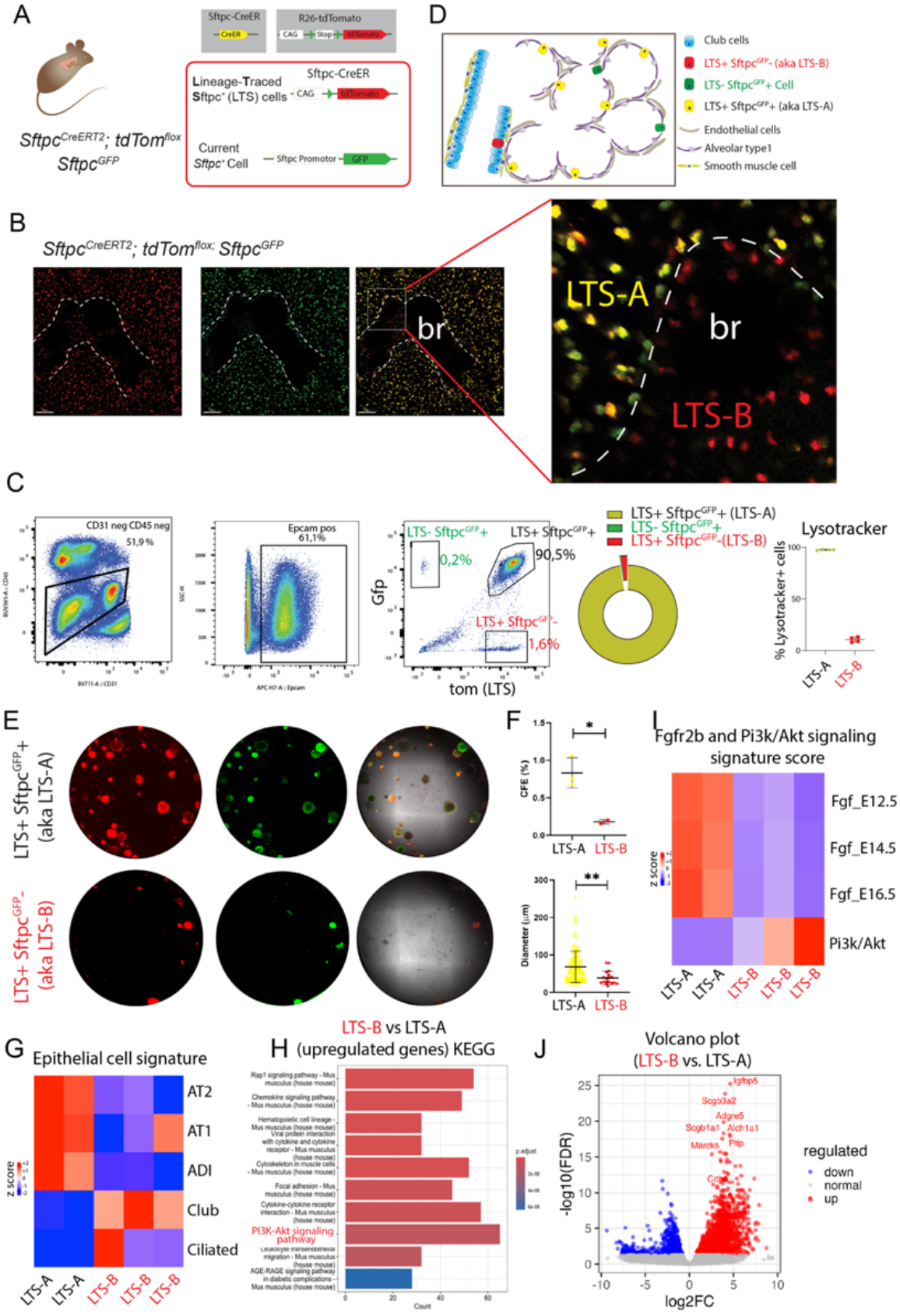
A
Sftpc-CreER
R26-tdTomato
Lineage-Traced Sftpc+ (LTS) cells
Current Sftpc+ Cell
Sftpc Promotor
GFP
Sftpc^CreERT2; tdTom^flox
Sftpc^GFP
D
Club cells
LTS+ Sftpc^GFP- (aka LTS-B)
LTS- Sftpc^GFP+ Cell
LTS+ Sftpc^GFP+ (aka LTS-A)
Endothelial cells
Alveolar type1
Smooth muscle cell
B
Sftpc^CreERT2; tdTom^flox; Sftpc^GFP
br
LTS-A
LTS-B
C
CD31 neg CD45 neg
51,9 %
Epcam pos
61,1%
LTS- Sftpc^GFP+
0,2%
LTS+ Sftpc^GFP+
90,5%
LTS+ Sftpc^GFP-
1,6%
Gfp
tom (LTS)
LTS+ Sftpc^GFP+ (LTS-A)
LTS- Sftpc^GFP+
LTS+ Sftpc^GFP-(LTS-B)
Lysotracker
% Lysotracker+ cells
LTS-A
LTS-B
E
LTS+ Sftpc^GFP+ (aka LTS-A)
LTS+ Sftpc^GFP- (aka LTS-B)
F
CFE (%)
Diameter (µm)
LTS-A
LTS-B
I
Fgfr2b and Pi3k/Akt signaling signature score
Fgf_E12.5
Fgf_E14.5
Fgf_E16.5
Pi3k/Akt
z score
G
Epithelial cell signature
AT2
AT1
ADI
Club
Ciliated
H
LTS-B vs LTS-A
(upregulated genes) KEGG
PI3K-Akt signaling pathway
Count
J
Volcano plot
(LTS-B vs. LTS-A)
-log10(FDR)
log2FC
regulated
down
normal
up

Figure 5: **Presence of a discrete population of tdTom+*Sftpc*GFP- population in the bronchial epithelium.**
A) *Sftpc*CreERT2 mice combined with Tomatoflox and *Sftpc*GFP mice were analyzed 14 days following tamoxifen IP administration. B) IF on the corresponding lung sections, showing that tdTom positive *Sftpc*GFP negative cells (in red only) are present in the bronchi. Notably that tdTom positive *Sftpc*GFP positive cells (the expected mature AT2s) are in yellow and located in the respiratory airways. C) FACS plot showing the presence of tdTom positive *Sftpc*GFP negative cells, which are negative for lysotracker. D) Schematic positioning of the different Lineage-traced *Sftpc*+ cells in the bronchi (LTS-B) and the alveoli (LTS-A) in the lung. E-F) Alveolosphere assays indicate that LTS-B, contrary to LTS-A, is quiescent. G) Epithelial signature on bulk RNA-seq of LTS-A and LTS-B, indicating that LTS-B shares common features with Club and Ciliated cells. H) LTS-B displays increased Pi3K/Akt signaling compared to LTS-A. I) LTS-B displays a low Fgfr2b signaling score compared to LTS-A. J) Volcano plot showing the most differentially expressed genes between LTS-B and LTS-A. Scale bar B: 150mm

4.3 scRNA-seq analysis of LTS-B reveals the presence of two subpopulations

Next, we investigated the potential heterogeneous nature of the LTS-Bs by carrying out scRNA-seq from sorted LTS-B cells in non-injured lungs (Figure 6A). The corresponding UMAP revealed the presence of two transcriptionally distinct populations (Figure 6B), one expressing the ciliated marker *FoxJ1* and *Tpp3* (Cluster 1) and one expressing the alveolar epithelial markers *Sftpc* and *Abca3* (Cluster 2). Interestingly, Cluster 1 also expressed a higher level of *Krt8* and *Krt18*, two bona fide ADI markers (Figure 6C), suggesting partial activation of Cluster 1 toward an injury-response state even in baseline conditions.

The heatmap in Figure 6D expands on the list of differentially expressed genes between these two clusters and supports that Cluster 1 displays ciliated-like cell characteristics and Cluster 2 displays AT2-like cell characteristics (Figure 6D). To further support the identity of these two clusters, we took advantage of the published scRNA-seq from Strunz et al. (Strunz et al., 2020). displaying most of the different epithelial cell clusters in the mouse lung (Figure 6E). Integration of the LTS-B scRNA-seq data with this dataset and the expression of key differentiation markers confirmed that Cluster 1 represents ciliated-like cells and Cluster 2 represents AT2-like cells (Figure 6F, G).

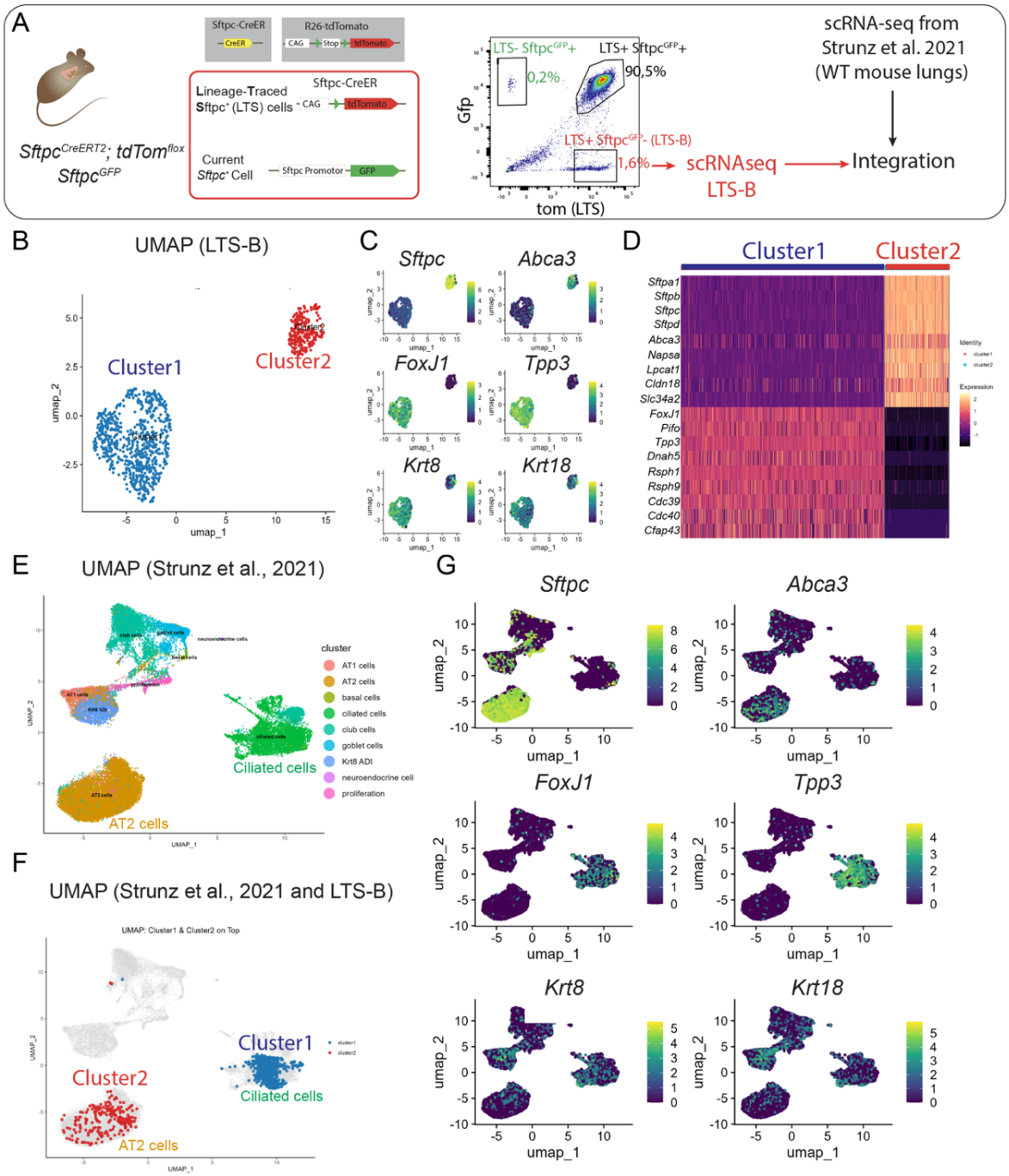

Figure 6: scRNA-seq on LTS-B indicates two subpopulations.
A) scRNA-seq experiments from LTS-B isolated from *Sftpc*CreERT2 mice combined with Tomatoflox and *Sftpc*GFP mice (analyzed 14 days following tamoxifen IP administration) were carried out and analyzed either directly (B-D) or integrated with the previously described mouse lung scRNA-seq dataset from Strunz et al (2020) to further define the identity of the LTS-B subclusters (E-G). (B-D) UMAP on LTS-B showing the presence of two distinct clusters called 1 and 2. Cluster 1 is enriched in ciliated markers *FoxJ1* and *Tpp3*, while Cluster 2 expresses AT2 markers *Sftpc* and *Abca3*. E) UMAP for the mouse lung epithelial cells from (Strunz et al., 2020). F) UMAP integrating the scRNA-seq data from LTS-B and (Strunz et al., 2020)showing that Cluster 1 is assigned with the ciliated cell identity, while Cluster 2 displays AT2-like characteristics. G) Expression of ciliated and AT2 markers in the integrated UMAP confirms the clusters' identity.

4.4 LTS-B are amplified in vivo following naphthalene injury and in vitro upon PCLS culture

Next, *Sftpc*CreERT2/+; tdTomatoflox/flox mice previously exposed to tamoxifen were subjected to naphthalene (NA) IP administration to damage the bronchial epithelial cells (Figure 7A, B).

Oil-treated control mice displayed only a few LTS-B cells, easily identifiable within the SMA staining in the bronchi (Figure 7C, upper panel, see also Figure 8A for higher magnification), and almost no proliferative cells in the bronchi (Figure 7C, lower panel). Note that most of the LTS-B cells did not display Scgb1a1 staining. By contrast, upon NA administration, a significant amplification of the LTS-B cells was observed at d5 (Figure 7D, upper panel. See also Figure 8B) and was associated with proliferation detected by EdU staining (Figure 7D, lower panel). Patchy Scgb1a1 expression was detected, confirming the NA-induced damage, and only a few tdTom+ cells in the airways expressed Scgb1a1. Quantification of the area occupied by LTS-B in the bronchial area confirmed the increased number of LTS-Bs in NA vs Oil (Figure 7E).

Next, we took advantage of our previously described PCLS injury model to look at the fate of the LTS-A and LTS-B cells over time. In our conditions, LTS cells are labeled in vivo with tamoxifen injection into the mice before processing the lungs for PCLS, followed by in vitro culture with live imaging for up to 185 hours (Figure 7F). Figure 7G shows that most of the LTS-A cells disappear within the first 24 hours of culture, as previously reported (Ahmadvand et al., 2021). This result was independently confirmed using PCLS from *Sftpc*GFP mice. By contrast, LTS-Bs were being amplified and displayed an invasive, migratory phenotype. Figure 7H displays the general quantification of the area occupied by the fluorescent signal, as well as the intensity of the signal in the bronchus area and alveolar area over time. Our results confirm the increase in LTS-Bs. Interestingly, in the alveolar area, the area occupied by the tdTom signal abruptly decreases within the first 8 hours and reaches a minimal value at 56 hours before increasing again and reaching a plateau at 140 hours before decreasing again. This dynamic pattern could be due to the migration of LTS-Bs in the alveolar area or the local amplification of the IAAPs as previously described (Ahmadvand et al., 2021), and data not shown. The graphical abstract in Figure 7I summarizes what is known so far about the LTS-B.

IF for Scgb1a1 in PCLS at 168 hours indicated a complete loss of the expression of this mature club cell marker, supporting major injury to the bronchial epithelium at this time (Figure 7J).

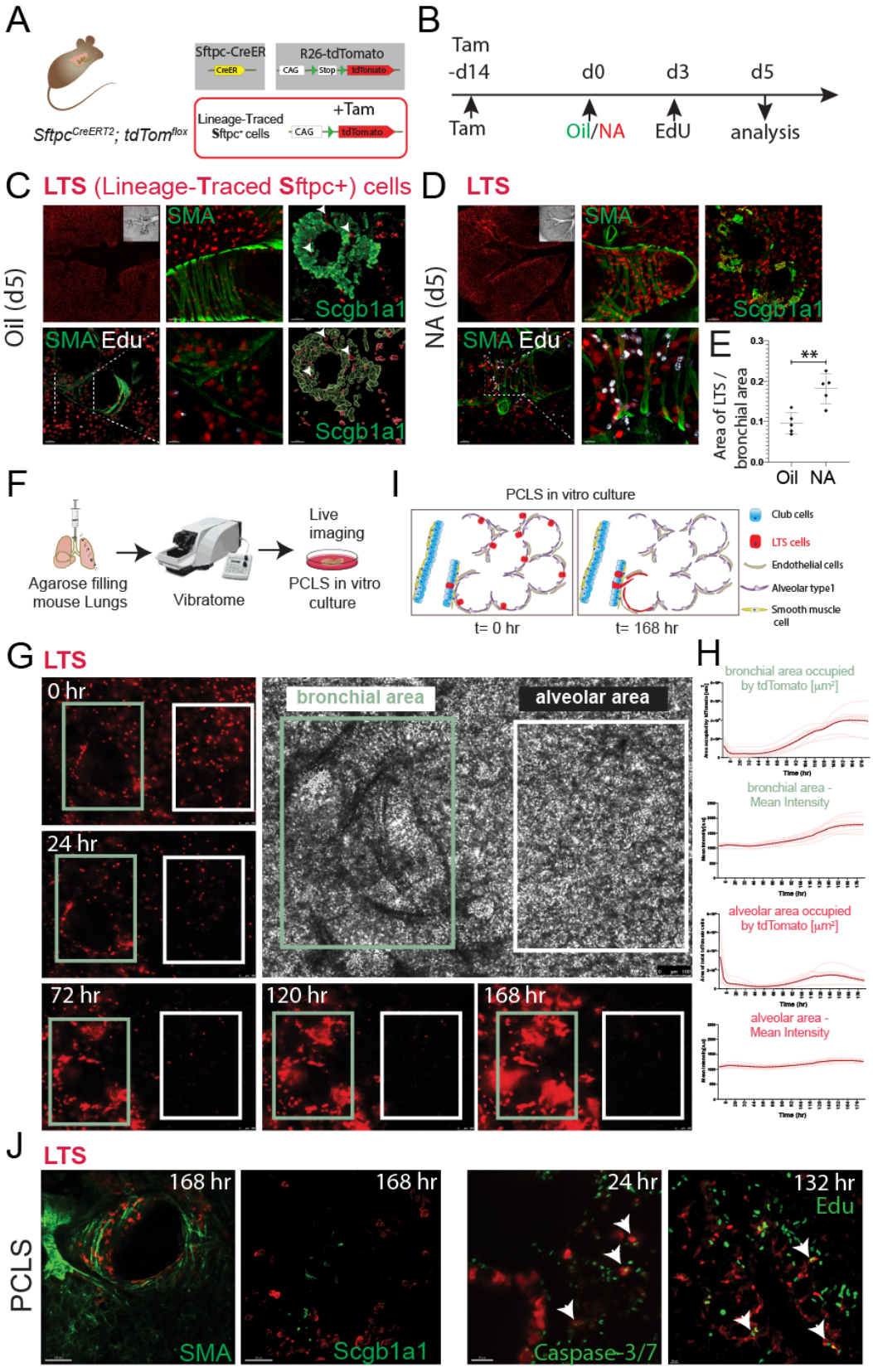

Figure 7: **LTS-Bs are amplified upon injury, either in vivo or in vitro.**
A-B) *Sftpc^{CreERT2}; tdTom^{flox}* female mice (n=10) were treated with tamoxifen to label the LTS-B in the bronchi and subjected to oil (control, n=5) or naphthalene IP injection (n=5) to trigger damage to the bronchial epithelium. Mice were injected with EdU on day 3 and sacrificed at day 5. C) Representative IF for tdTom, SMA, Scgb1a1, and EdU in Oil at day 5. D) Representative corresponding IF staining on the lungs of NA-treated animals. E) Quantification of the area occupied by tdTom+ cells in the bronchi (Each dot represents the mean of three randomly selected bronchial regions), confirming the amplification of LTS-B cells. F) *Sftpc^{CreERT2}; tdTom^{flox}* mice (n=3) were injected with tamoxifen 2 weeks before sacrifice, and the corresponding lungs were processed for PCLS. G) Representative fluorescent images of LTS cells in the bronchial area (LTS-B cells) and alveolar areas (LTS-A cells) of PCLS (n=3 from 3 independent mice) at different time points. H) Quantification of the mean area occupied by LTS-B and LTS-A and associated mean fluorescence intensity in the bronchiolar and alveolar areas of PCLS over time (the line in bold represents the mean of 11 Individual faint lines. Each faint line representing the area and fluorescence intensity of a randomly selected bronchiolar and alveolar area over 3 independent PCLS (1 PCLS/mouse). I) Schematic illustrating the changes observed in the PCLS over time. J) Representative SMA and Scgb1a1 staining at 168 hrs. Caspase 3/7 and live-dead staining of PCLS after 24 hours of culture. EdU staining of PCLS after 132 hours of culture. Scale bar C, D: 50 μm, G: 100 μm, J: 100 μm 50 μm 30 μm 30 μm.

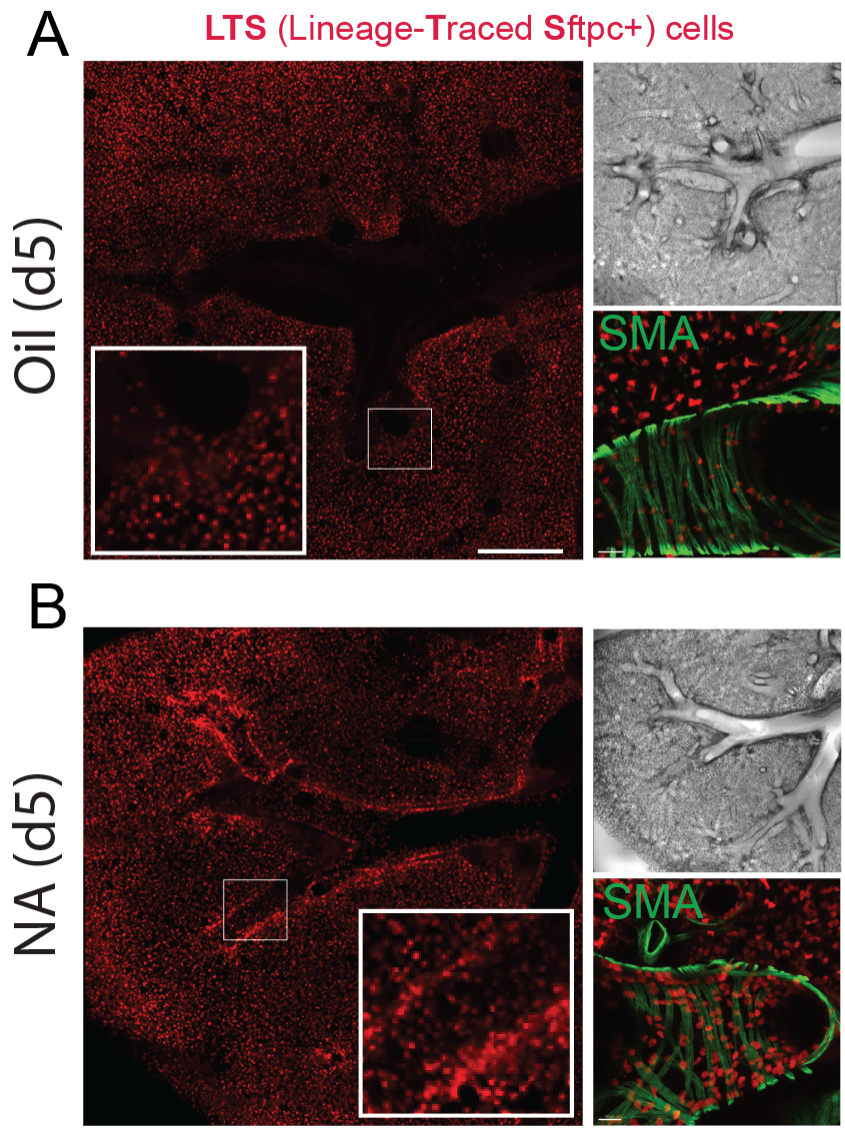

Figure 8: Amplification of the LTS-B upon NA exposure.
A) Oil-treated control mice at d5 displayed only a few LTS-B cells, easily identifiable within the SMA staining in the bronchi. B) NA-treated mice showing amplification of LTS-B within the SMA staining in the bronchi.

4.5 Characterization of LTS cells isolated from PCLS at 168 hours suggests that LTS-Bs adopt a transitional state towards the AT2 lineage

We used FACS to isolate LTS cells from the PCLS at 168 hours of culture (called LTS-PCLS) and carried out scRNA-seq (Figure 9A). We integrated the LTS-PCLS and LTS-B cells dataset previously generated (Figure 9B). Three clusters were identified. Clusters 1 and 2 correspond to the Ciliated-like cells and AT2-like cells present in LTS-Bs, while Cluster 3 appears only with the LTS-PCLS cells dataset.

These results were confirmed through the expression and quantification of specific markers for AT2s, Ciliated cells, and ADI on the UMAP and associated violin plots (Figure 9B).

Integration with the Strunz et al. dataset identifies Cluster 3 as the Krt8-ADI subpopulation (Figure 9C). These results were confirmed through heatmap visualization using groups of specific markers for each subpopulation (Figure 9C). IF staining for LTS-PCLS cells for *Krt8* and *Krt18* confirms the ADI identity of Cluster 3 (Figure 9D). We also integrated human scRNA-seq data from healthy and IPF lung samples using the dataset from Habermann et al. (2020) and our mouse scRNA-seq data (Figure 4E). Here, we also observed similarities to AT2 cells and ciliated cells. Notably, in the LTS-PCLS group, the highest similarity was found in $KRT5^{-}/KRT17^{+}$ basaloid cells.

We have also compared using bulk RNA-Seq from sorted LTS-PCLS and LTS from the non-injured lung (containing LTS-A and LTS-B) (Figure 11). Our results confirmed the ADI identity of the LTS-PCLS (Figure 11B), the sustained activation of Pi3k/Akt (Figure 11C, D). Identification and analysis of differentially expressed genes between these three clusters is shown in the heatmap and KEGG analysis in Figure 10. KEGG analysis indicates that Cluster 2 is enriched in lipid metabolism, Ampk signaling, and Pi3k signaling, reflecting the AT2-like nature of these cells, while Cluster 3 is enriched in actin cytoskeleton organization, focal adhesion, and integrin-mediated cell signaling and cell motility, reflecting the migratory behavior of these cells in PCLS.

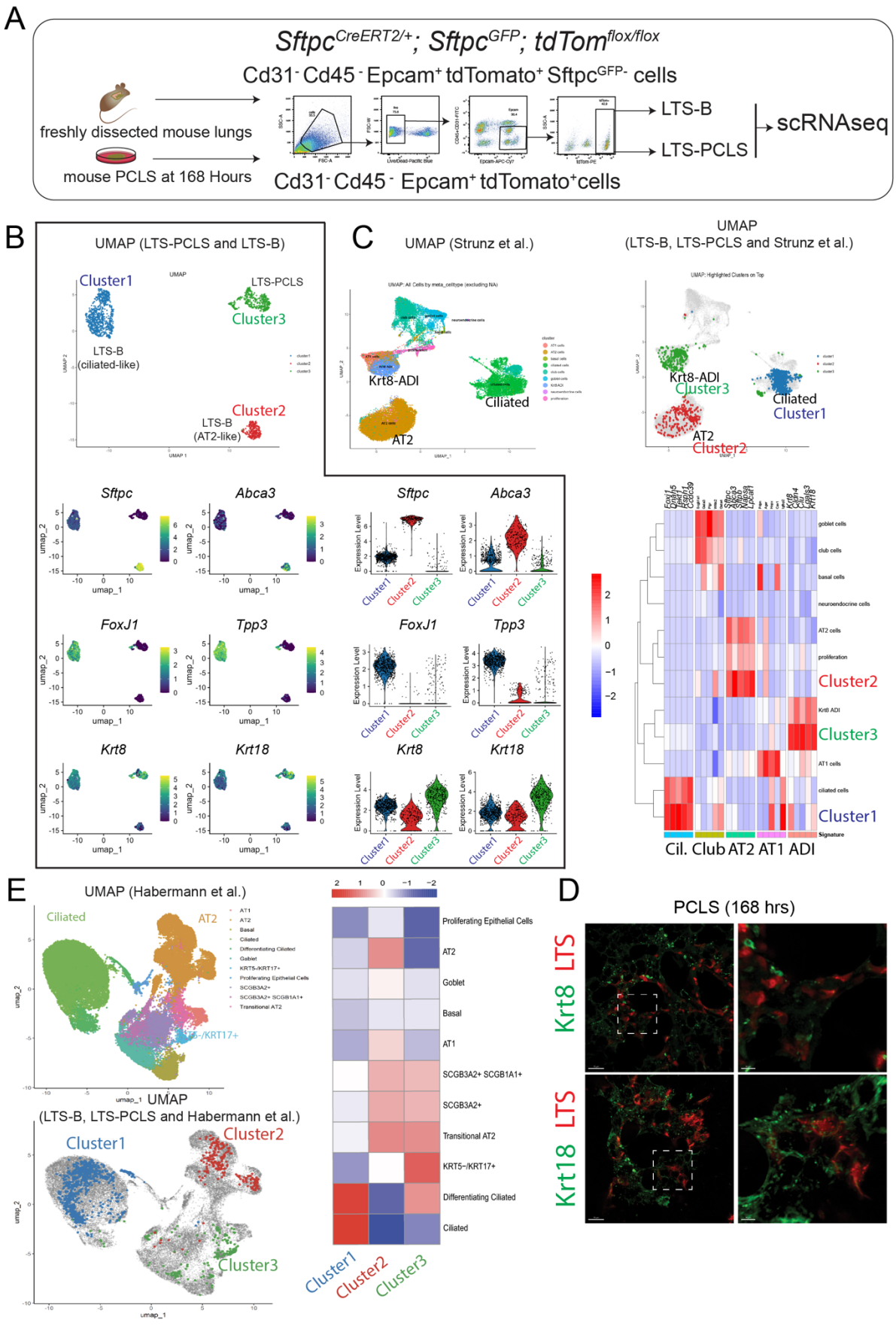
A
Sftpc CreERT2/+; Sftpc GFP; tdTom flox/flox
Cd31- Cd45- Epcam+ tdTomato+ Sftpc GFP- cells
freshly dissected mouse lungs
mouse PCLS at 168 Hours
LTS-B
LTS-PCLS
scRNAseq
Cd31- Cd45- Epcam+ tdTomato+cells
B
UMAP (LTS-PCLS and LTS-B)
Cluster1
LTS-PCLS
Cluster3
LTS-B
(ciliated-like)
Cluster2
LTS-B
(AT2-like)
Sftpc
Abca3
FoxJ1
Tpp3
Krt8
Krt18
C
UMAP (Strunz et al.)
Krt8-ADI
Ciliated
AT2
UMAP
(LTS-B, LTS-PCLS and Strunz et al.)
Krt8-ADI
Cluster3
Ciliated
Cluster1
AT2
Cluster2
goblet cells
club cells
basal cells
neuroendocrine cells
AT2 cells
proliferation
Cluster2
Krt8 ADI
Cluster3
AT1 cells
ciliated cells
Cluster1
Signature
Cil. Club AT2 AT1 ADI
E
UMAP (Habermann et al.)
Ciliated
AT2
KRT5-/KRT17+
UMAP
(LTS-B, LTS-PCLS and Habermann et al.)
Cluster1
Cluster2
Cluster3
Proliferating Epithelial Cells
AT2
Goblet
Basal
AT1
SCGB3A2+ SCGB1A1+
SCGB3A2+
Transitional AT2
KRT5-/KRT17+
Differentiating Ciliated
Ciliated
D
PCLS (168 hrs)
Krt8 LTS
Krt18 LTS

Figure 9: LTS isolated from PCLS at 168 hr adopts an ADI signature.
A) sorted LTS-PCLS were processed for scRNA-seq, and the data were integrated with the scRNA-seq from LTS-B. B) UMAP showing the integration of the 2 datasets, indicating the presence of the previously described ciliated-like (Cluster1) and AT2-like (Cluster2) populations present in LTS-B. An additional population corresponding to LTS-PCLS (Cluster3) is identified. C) These data are integrated with the Strunz et al dataset for the annotation of the populations. Our results indicate that Cluster3 matches with the Krt8+ADI. D) Expression on the UMAP of AT2 markers (*Sftpc*, *Abca3*), ciliated markers (*FoxJ1, Tpp3*), and ADI markers (*Krt8, Krt18*), as well as the corresponding quantification for these genes for each cluster. E) heatmap showing the top 5 markers for each cell type, further confirming the identity of clusters 1, 2, and 3. F, G) Heatmap of the top 100 genes and corresponding GO/KEGG enrichment analysis for Clusters 2 and 3. H) IF for Krt8 and 18 showing the expression of these ADI markers in LTS-PCLS. Scale bar H: 70 mm

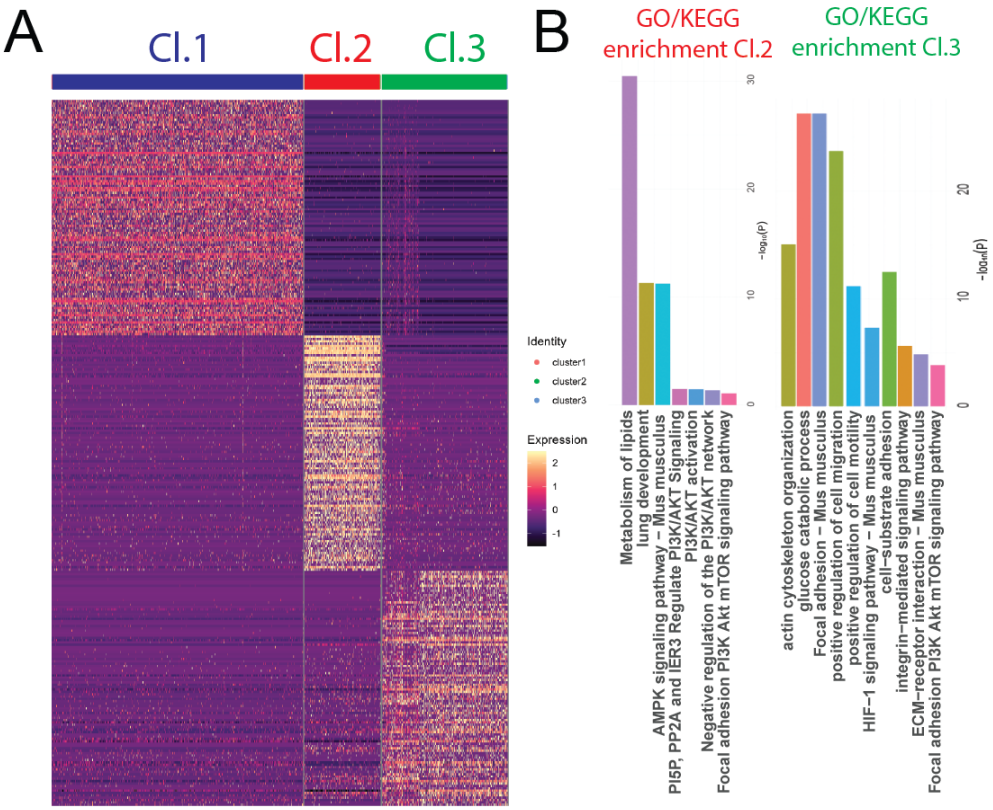

Figure 10: Characterization of clusters 1, 2, and 3 identified in native lungs and in LTS-PCLS.
A) heatmap showing the top 100 genes for each cluster. B) Corresponding GO/KEGG enrichment analysis for Clusters 2 (AT2-like) and 3 (LTS-PCLS).

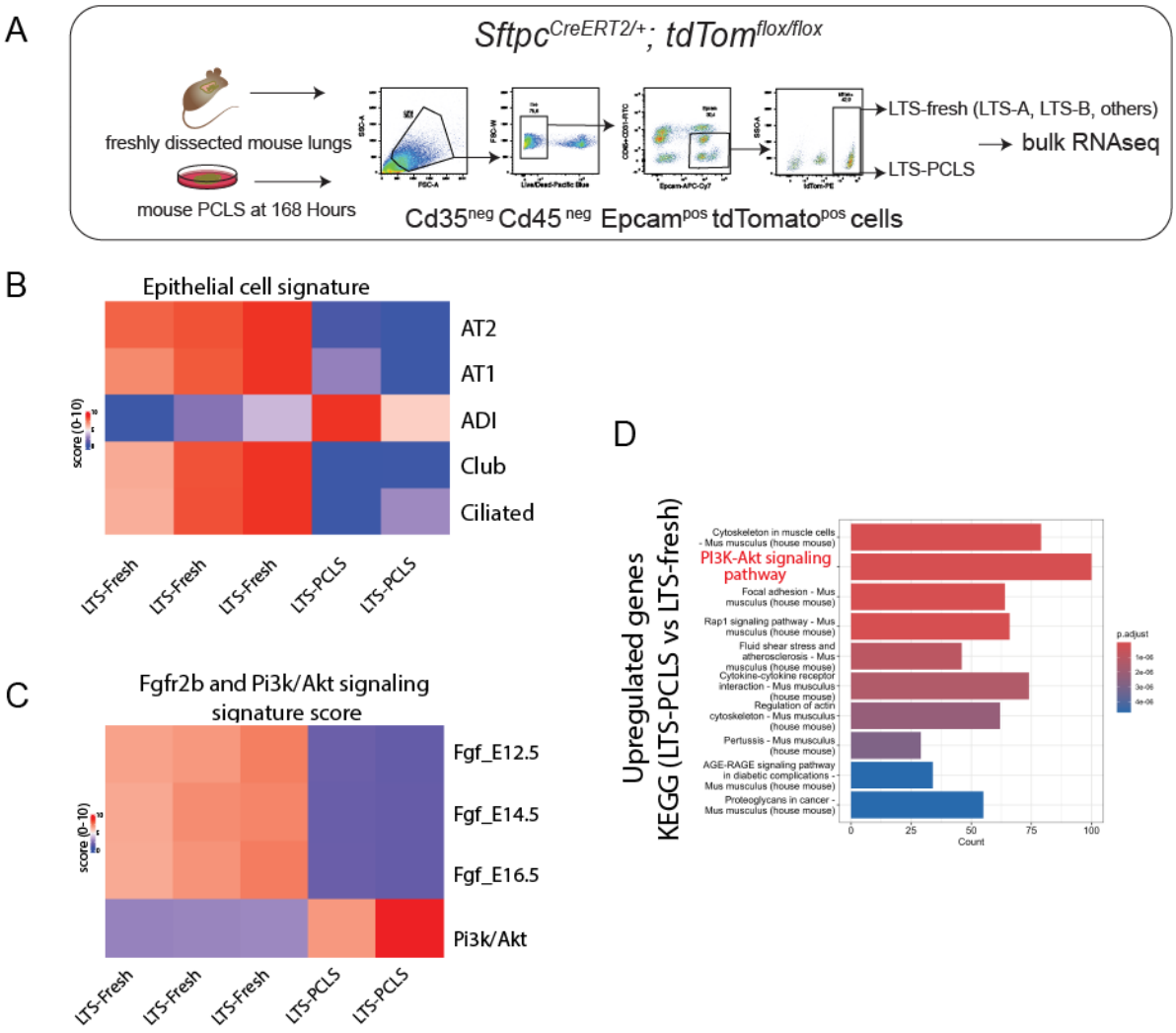

Figure 11: Characterization of LTS cells after culturing PCLS reveals the presence of ADI transcript with upregulation of the Pi3k/Akt pathway.
A) LTS cells from *Sftpc*CreERT2 mice combined with Tomatoflox were sorted with FACS in native lungs (LTS-fresh) and after 8 days of PCLS culture (LTS-PCLS) and processed for bulk RNA-seq. B) Epithelial signature on bulk RNA-seq of LTS-PCLS and LTS-Fresh, indicating that LTS-PCLS shares common features with ADI. C) LTS-PCLS displays a low Fgfr2b signaling score compared to LTS-Fresh. D) LTS-PCLS displays increased Pi3K/Akt signaling compared to LTS-Fresh.

4.6 LTS-B cells differentiate into *Sftpc*^{GFP} positive cells upon treatment with FGF10 and CHIR99021

As our scRNA-seq indicated that LTS-B cells displayed characteristics of ADI, we wondered how LTS-PCLS cells would behave when cultured in conditions known to trigger AT2 differentiation. To trigger commitment of the LTS-B towards the AT2 lineage, PCLS from *Sftpc*CreERT2 mice combined with Tomatoflox were treated or not with a mixture of FGF10 (3ng/mL) and Wnt agonist CHIR99021 (3µM).

First, we validated our experimental conditions using the *Sftpc*CreERT2 mice, which have been previously described to be leaky(Ahmadvand et al., 2021). We first examined the fluorescent signal for LTS-PCLS in PCLS arising from mice not exposed to tamoxifen. Our results indicate that under these conditions, the fluorescent signal for LTS-PCLS over time (2h, 48h, and 168h) was not observed (Figure 12C). In addition, examination of the fluorescent signal in non-injured lungs of *Sftpc*CreERT2 mice not exposed to tamoxifen indicates the presence of only 0.2% LTS-B (out of total tdTom, data not shown) compared to the previously described 1.6% LTS-B in the presence of tamoxifen. This result suggests that the previously observed leakiness in this line captures mostly the LTS-A and not the LTS-B cells. The addition of FGF10 and CHIR to the culture medium of the PCLS does not significantly change this result. Figure 12F, G displays the quantification of the area occupied by LTS- PCLS at 2 hours and 168 hours in the different experimental conditions.
The addition of tamoxifen in vitro (PCLS Tam) resulted in only a few LTS-PCLS in the bronchi being labeled, suggesting that the LTS-B to LTS-PCLS transition also led to a decrease in their differentiation towards AT2s. However, upon addition of FGF10+CHIR, the fluorescent signal for LTS-B was increased (Figure 12D, F, G).
By contrast, upon tamoxifen exposure in vivo (Tam PCLS), an increased signal for LTS-PCLS in the bronchi was observed at all time points examined (Figure 12E).

Next, we used the *Sftpc*CreERT2 mice combined with Tomatoflox and *Sftpc*GFP to track the dynamic differentiation of the LTS-B using live imaging (Figure 13A). Figure 13B shows the graphical abstract of the different and relevant epithelial cells for our study.
Figure 13C shows representative low-magnification pictures of PCLS in the absence (control) or presence of FGF10 or FGF10+CHIR. Our results indicate that in the presence of FGF10 and CHIR, LTS-B acquired *Sftpc*GFP expression in the bronchial area. Note also the cumulative effect of the combined treatment compared to FGF10 alone.
The quantification of the tdTom and GFP area in the bronchial and alveolar areas over time is shown in Figure 13D. Note the absence of GFP signal in the alveolar area, in sharp contrast with the robust response in the bronchial area.

Figure 13E shows high magnification of the bronchi in control and experimental conditions, confirming the presence of tdTom-positive and *Sftpc*GFP positive cells (labeled in yellow). Please note that not all the LTS-B cells are yellow, indicating an incomplete response of LTS-B cells and revealing a potential heterogeneity in this progenitor population.

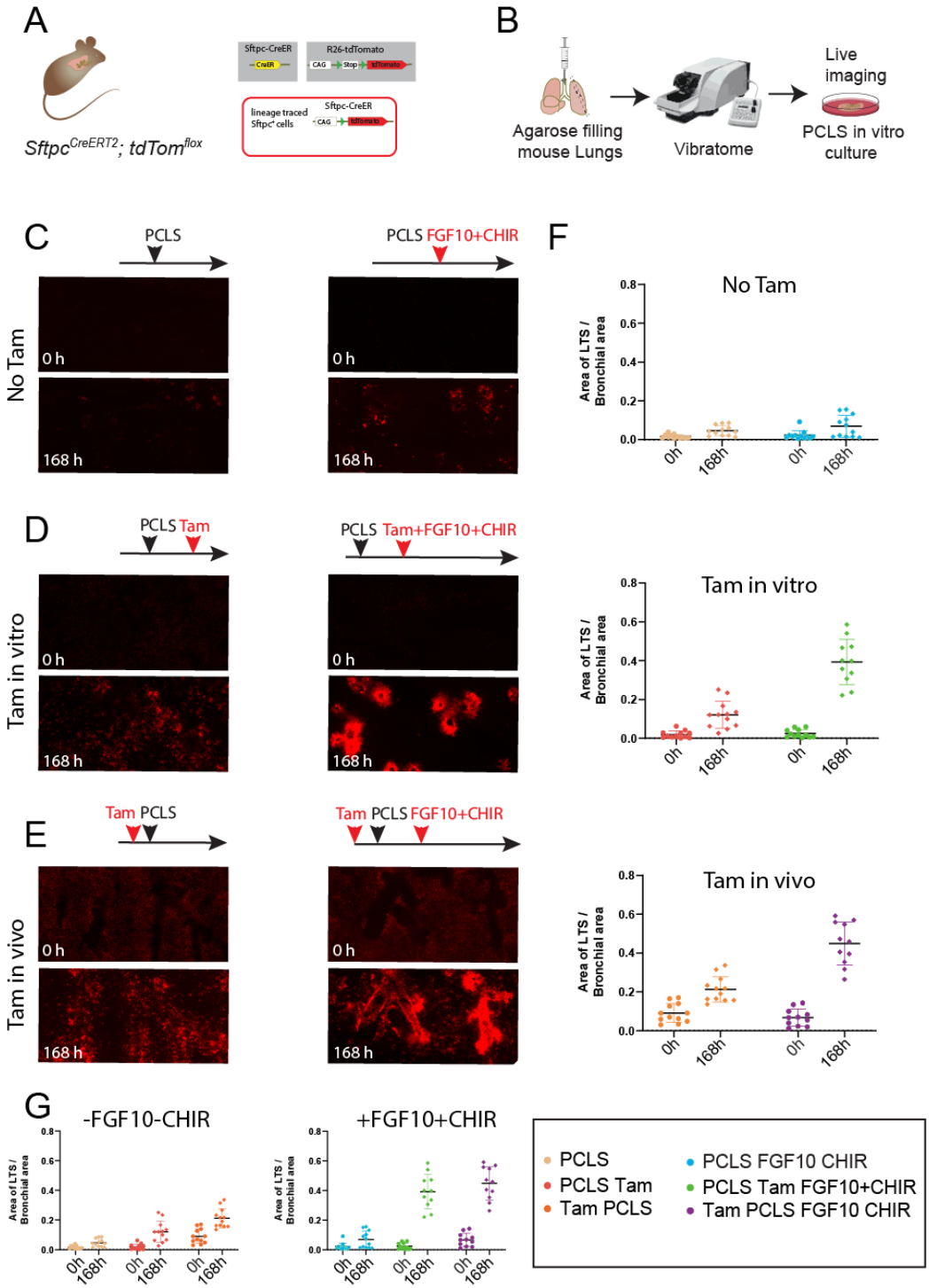

Figure 12: Quantification of LTS-PCLS in bronchial area in absence or presence of FGF10+CHIR. A, B) PCLS were prepared from *Sftpc*CreERT2 tdTomflox lungs. C-E) Representative IF pictures of PCLS at time 0 and 168 hours in different timing of tamoxifen treatment and in the presence or absence of FGF10+CHIR. C) In the absence of Tam treatment, LTS-B are not visible at 168 hours. Upon FGF+CHIR treatment, a modest increase in LTS-B is observed. D) Tam administration in vitro leads to a small increase in LTS-B at 168 hours. FGF10+CHIR treatment leads to a significant increase in LTS-B in the bronchial area. E) Tam administration in vivo leads to a robust increase in LTS-B compared to the one observed for Tam administration in vitro. A solid increase in LTS-B presence is observed upon treatment with FGF10+CHIR. F) Quantification of the area of LTS-B in the bronchial area under different tam administration conditions. G) Quantification of the area of LTS-B in the bronchial area in absence or presence of FGF10+CHIR.

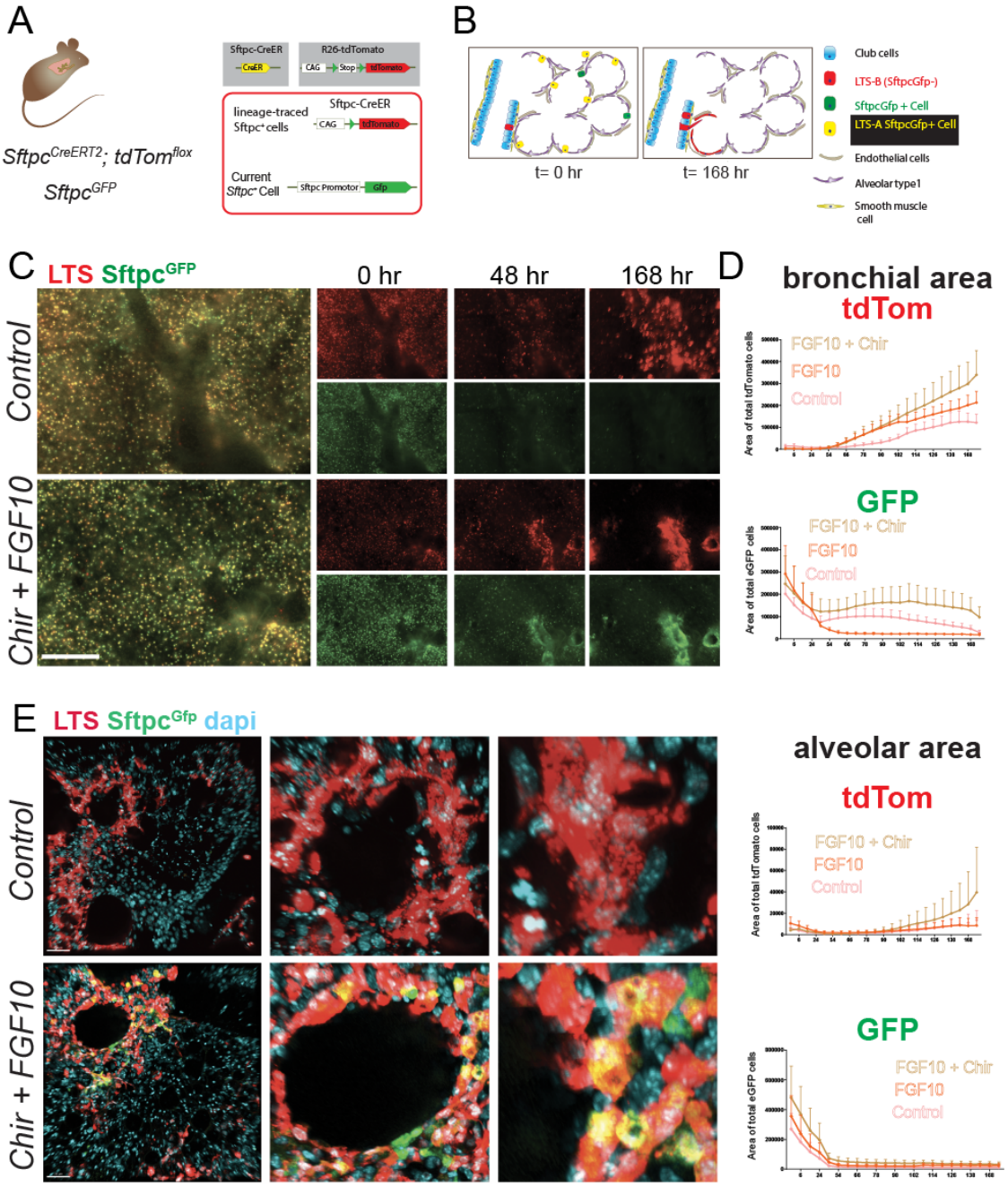

Figure 13: **LTS-B cells partially differentiate into *Sftpc*GFP positive cells upon treatment with FGF10 and CHIR99021.**
A) *Sftpc*CreERT2 mice combined with Tomatoflox and *Sftpc*GFP mice were used to generate PCLS. B) Schematic of the position of the different cells of interest. C) IF for tdTom and *Sftpc*GFP on PCLS sections in control and CHIR+FGF10 conditions. Note the presence of LTS-B, which expresses *Sftpc*GFP positive upon CHIR+FGF10 treatment. D) Quantification of tdTom and GFP in bronchial and alveolar areas over time, respectively. E) High magnification of PCLS sections shown in C. Note the abundant presence of LTS-B *Sftpc*GFP+ cells (in yellow) in the bronchi upon FGF10+CHIR treatment. Note also the presence of Tom-*Sftpc*GFP+ (green only) as well as Tom+*Sftpc*GFP- (red only). Scale bar C: 200 mm, E: 250 mm, H: 70 mm.

4.7 Live confocal movie analysis and scRNA-seq confirm that LTS-PCLS cells get committed to the AT2 lineage

Next, we carried out live confocal imaging on PCLS from *Sftpc*CreERT2; tdTomflox; *Sftpc*GFP to gain more insight into the acquisition of *Sftpc*GFP expression by LTS-B ADI cells (Figure 14). In the absence of FGF10/CHIR in the PCLS, we confirmed the loss of LTS-A cells (in yellow) and the amplification of LTS-B cells (in red) (Figure 14A, see Supp Movie 3). By contrast, in the presence of FGF10/CHIR, we observed the appearance of abundant *Sftpc*GFP cells (green only) as well as LTS-ADI cells that had acquired *Sftpc*GFP expression (yellow) (see Supp Movie 4). Similar to what was observed with the experiment in the absence of CHIR/FGF10, we observed the loss of LTS-A cells (Figure 14B).

To confirm that LTS-ADI cells acquired *Sftpc*GFP, we carried out a digital section of a LTS-ADI *Sftpc*GFP+ cell and confirmed the absence of nearby *Sftpc*GFP+ cells that could have confounded our interpretation (Figure 14C). Next, we isolated LTS-PCLS cells cultured in the presence of FGF10/CHIR (LTS-PCLS-Exp) and carried out scRNA-seq experiments (Figure 14D). Integration with the LTS-PCLS-Ctrl cells previously generated indicated the presence of four clusters (Clusters a-d). Under the action of FGF10/CHIR, we observed that most of the LTS-B ADI cells were present in Cluster C. (Figure 14E, see distribution). Expression of AT2 markers on the UMAP confirmed that Cluster c was enriched in *Sftpc* and *Abca3*. The heatmap for the expression of differentially expressed genes indicates the enrichment of AT2 genes in Cluster c specifically (Figure 14F), confirming the differentiation of LTS-B ADI to the AT2 lineage in the presence of CHIR/FGF10.

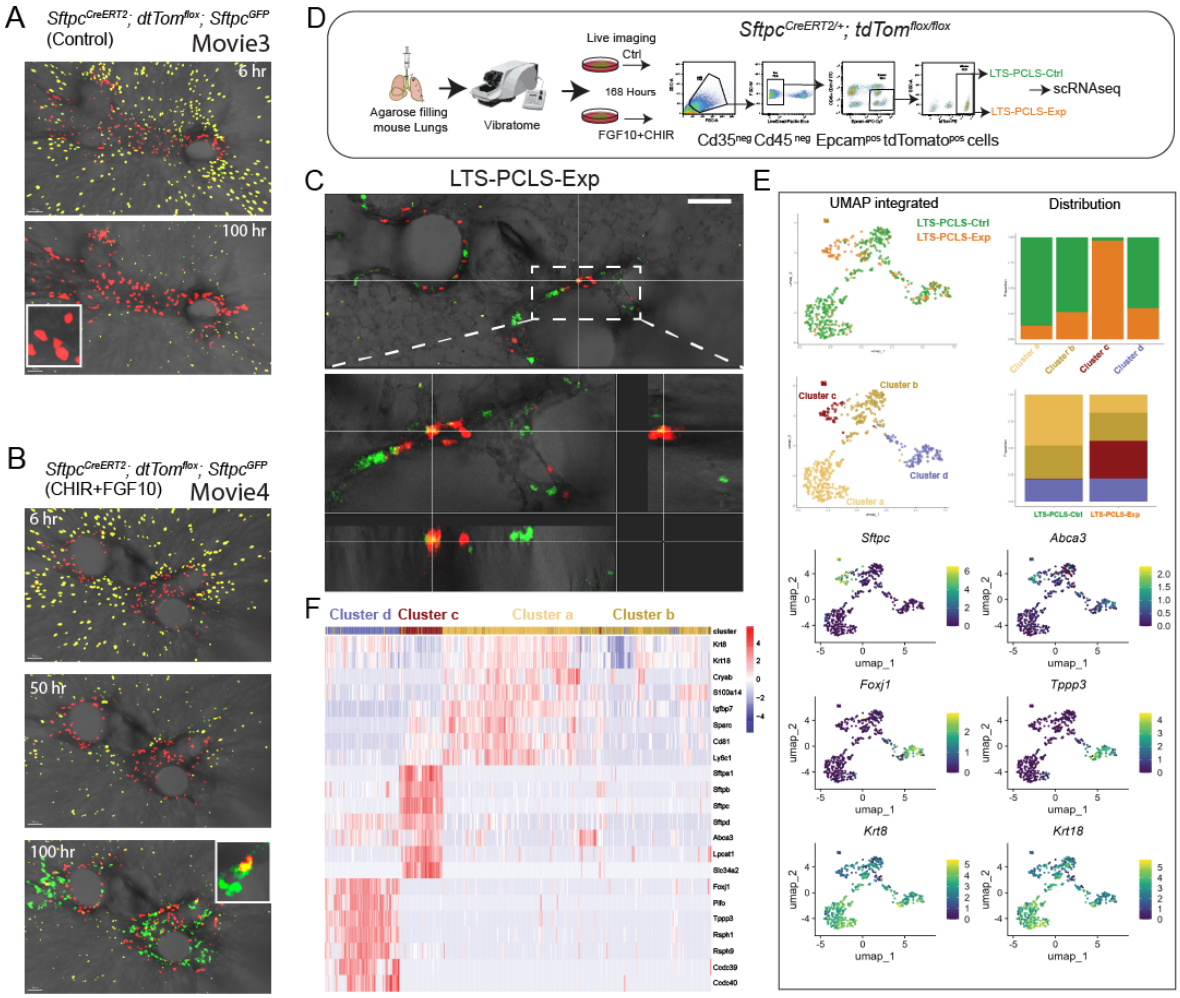

Figure 14: **Impact of CHIR+FGF10 treatment of PCLS on LTS-B from *Sftpc*CreERT2, tdTomflox; *Sftpc*GFP mice.**

A-B) Image capture from confocal movies in the absence or presence of CHIR+FGF10. Note in A, the disappearance of LTS-A and the amplification of LTS-B over time. Note that in the presence of FGF10+CHIR, a similar loss of LTS-A is observed, but some of the LTS-B have acquired *Sftpc*GFP expression (yellow cells). In addition, note the abundant presence of LTS-*Sftpc*GFP+ cells. C) Digital section in the X, Y, and Z axis showing that this cell is not surrounded by any other *Sftpc*GFP cells and that the GFP signal is inside the tdTom+ cells. D) Schematic approach to generate scRNA-seq data from PCLS cultured for 168 hr in normal medium or medium containing FGF10+CHIR. E) Integrated UMAP for LTS-PCLS-Ctrl and LTS-PCLS-Exp, allowing the identification of 4 subclusters. Distribution analysis indicates that Cluster c is made mostly of cells arising from LTS-PCLS-Exp, suggesting that this cluster is the result of FGF10-CHIR activity. Expression of *Sftpc* and *Abca3* is enriched in Cluster c compared to the other clusters. Cluster C is enriched for markers of the AT2 lineage. Cluster d is enriched in markers of the ciliated lineage, while Clusters a and b are enriched in ADI markers. F) Heatmap showing the enrichment of marker genes for the ciliated cells, AT2 cells, and ADI cells in the corresponding clusters. Scale bar: B: low mag: 60 mm, high mag: 20 mm.

4.8 LTS-B cells and BASCs represent two independent populations

As our results indicated that over the time course of the PCLS culture, these cells accumulate in the distal part of the bronchi (See Supp Movie 1 and 2 and Figure 15A, B), we investigated whether the LTS-B cells could have similarities with BASCs. In

order to examine the behavior of BASCs in PCLS, we used the previously described BASC tracer and BASC viewer mice (Salwig et al., 2019) based on the use of split-Cre or split-tTA, respectively (Figure 15C, D, and E, F). Our results indicate that in PCLS cultured in medium, the tracer, which permanently labels BASCs, shows only discrete cells at the BADJ at day 0 and day 3, and a complete absence of the lineage-labeled cells at day 8. Similar results were obtained with the viewer, which allows detection of the BASCs at the time of staining. By comparison, the PCLS cultured in the presence of the Wnt agonist CHIR and FGF10 displayed a robust amplification of the BASCs, visualized both using the tracer and the viewer. LTS-B cells are therefore independent of the BASCs, as already suggested by their rather broad presence along the bronchi as well as by the scRNA-seq results.

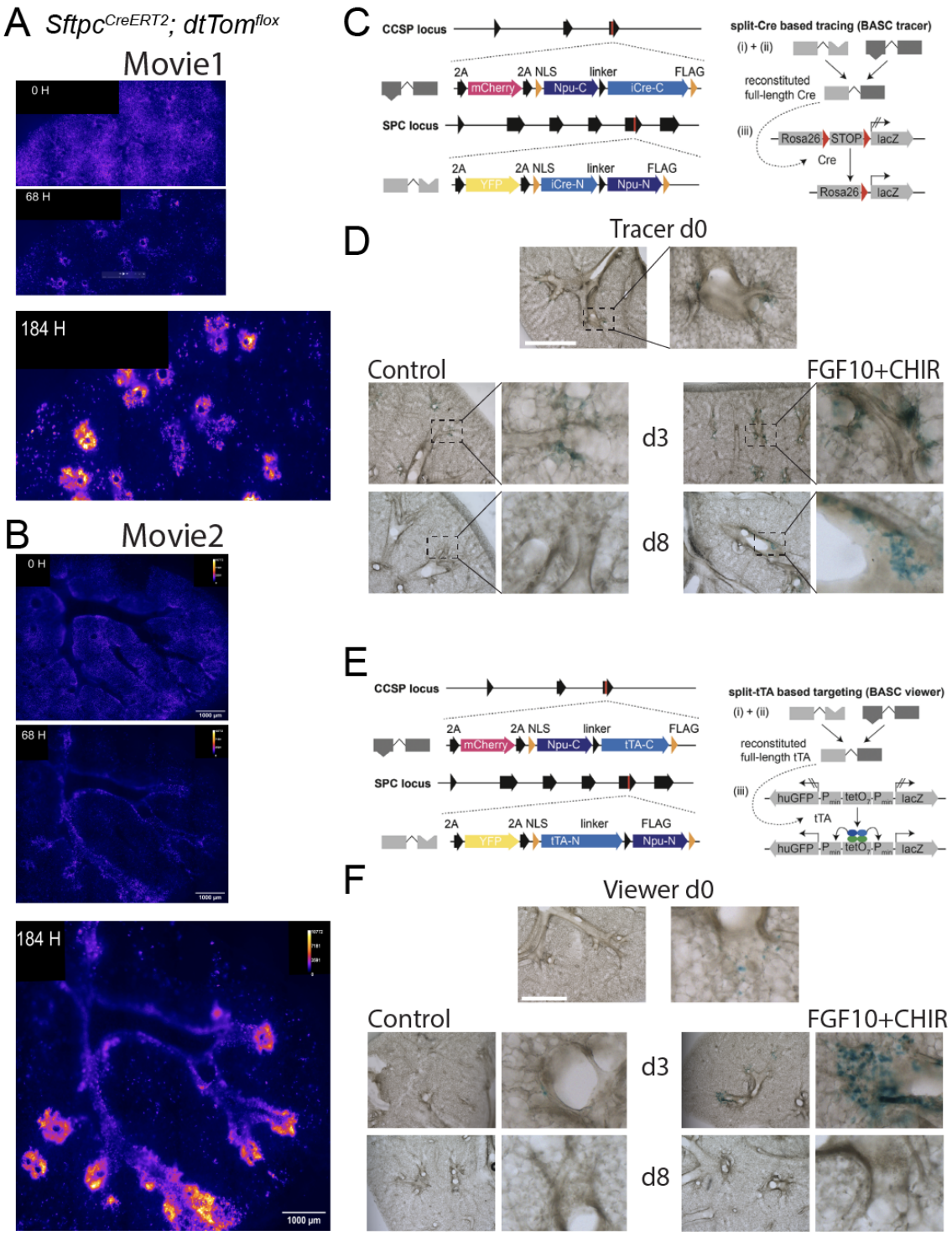

Figure 15: LTS-B are distinct from BASCs.
A, B) Live fluorescence microscopy of *Sftpc*CreERT2, tdTomflox lungs. Selected pictures over time showing the signal on cross sections (movie1) and longitudinal sections (movie2). Note that the tdTom+ cells accumulate in the distal part of the bronchi, where the BASC are also known to be present. C) Use of the BACSC tracer mice for Bronchoalveolar stem cells described in (Salwig et al., 2019). D) PCLS from these mice over time shows the presence of discrete BASC at BADJ at the time of lung processing for PCLS (d0). Upon PCLS culture, BASC are still detected at d3 but no longer visible at d8. However, BASC are amplified in PCLS in the presence of FGF10+CHIR both at d3 and d8. This suggests that the *Sftpc*+tdTom- likely corresponds to the BASC. E, F) Similar results are observed with the BASC viewer mice. Scale bar 1000 mm

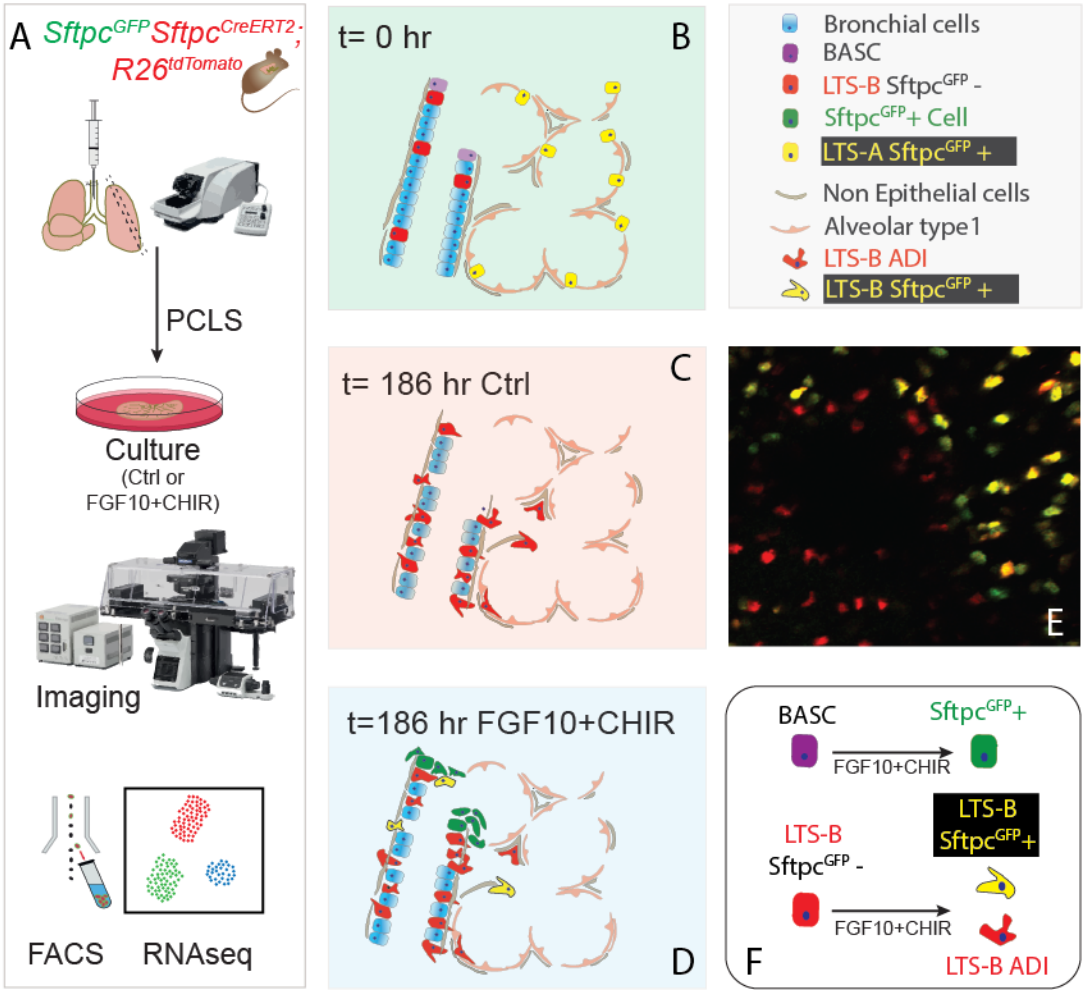

Figure 16: **graphical abstract**
*Sftpc*CreERT2 lineage tracing has been instrumental in defining alveolar epithelial heterogeneity. Using *Sftpc*CreERT2; Tomatoflox and *Sftpc*GFP mice combined with IF, FACS, RNA-seq, and live imaging, we identified two lineage-traced populations: alveolar *Sftpc*GFP+ AT2 cells (LTS-A) and bronchi-localized *Sftpc*GFP– cells (LTS-B). Upon injury in vivo or in PCLS, LTS-B cells expanded and migrated from the bronchi, adopting an alveolar differentiation intermediate (ADI)-like state. Treatment with FGF10 and CHIR99021 partially induced their differentiation into *Sftpc*GFP+ cells., LTS-B cells represent a distinct population from BASC upon Treatment with FGF10 and CHIR.

Chapter 5: Discussion

Using *Sftpc*CreERT2 mice combined with Tomatoflox and *Sftpc*GFP mice, in vivo naphthalene injury and in vitro cultured PCLS, as a new model of injury, we have identified a new population of epithelial progenitor cells for the alveolar lineage in the bronchi called LTS-B, distinct from club cells, LNEPs, BASCs, and AT2 cells. Upon injury, LTS-B cells acquire an ADI phenotype. We also present evidence that some of these cells gain *Sftpc*GFP expression upon exposure to FGF10 and CHIR.

5.1 In vitro culture of Precision-Cut Lung Slices (PCLS) to unravel the behavior of epithelial progenitor cells upon severe injury

A significant advantage of the PCLS model is that the three-dimensional architecture of lung tissue, including alveolar and airway structures, is preserved in culture over time. This was achieved by culturing PCLS in media that support the survival of the epithelial cells (Koziol-White et al., 2024). This approach has allowed us to characterize the behavior using live imaging of lineage-labeled AT2 cells in the alveoli (Chioccioli et al., 2024). PCLS can also be injured by elastase (emphysema model), bleomycin, or a fibrotic cocktail (fibrosis model). This model is therefore superior to traditional two-dimensional cultures, as the correct physiological function of the lung depends on this three-dimensional architecture, including the intercellular interactions. PCLS have been used for infectious disease studies as well as for projects related to toxicology, pharmacology, and immunology. As the PCLS approach allows generating multiple slices from a single lung, it reduces the number of animals needed for the experiments. Besides these applications, our study also demonstrates that the PCLS, in our culture conditions, serves as a model of severe lung injury combining massive and simultaneous damage to the conducting and respiratory airway. A preliminary investigation into the reasons behind such a strong injury observed in our PCLS culture conditions indicates that this is linked to the presence of agarose in the parenchyma. In our conditions, when a strong injury is observed, the lungs are systematically well inflated with the low-melting agarose solution. However, we noticed that suboptimal inflation of the lungs allows the AT2 cells in the PCLS to survive well beyond 184 hours. Therefore, the link between the amount of agarose present in the lung is an important parameter to consider in studies involving PCLS.

Interestingly, the severe damages observed in the alveolar compartment with a complete loss of AT2s, which occurs in the context of paraquat exposure, are associated with a high burden to the animals. Our model is therefore innovative and important in the context of the 3Rs.

5.2 LTS-B cells are distinct from existing BASCs, LNEP, basal-like/Club cells

Several progenitor cells for the alveolar lineage have been described in the bronchi. Rare p63+ basal-like cells, Sca1+ cells, or BASCs and Scgb1a1-traced cells, which are thought to be club cells, are all reported to expand and mobilize after injury to repair the alveolar epithelium (Kim et al., 2005; Liu et al., 2019; McQualter, 2019; McQualter et al., 2010; Vaughan et al., 2015b; Zuo et al., 2015)

Of interest for this study, BASCs are progenitor cells residing in the distal end of terminal bronchioles. BASCs express both club cell marker, Scgb1a1, and AT2 cell marker, *Sftpc*. In mice, they can regenerate both bronchiolar and alveolar epithelial cells following lung injury (Liu et al., 2019). However, in the context of the PCLS culture over time, BASCs are no longer detected (Figure 15), in sharp contrast with LTS-B cells.

Recently, a small population (around 5%) of club-like cells captured by the Scgb1a1CreERT2 driver and Lineage-Negative for *Sftpc* (using the *Sftpc*CreERT2 driver) Epithelial Progenitors (called LNEPs) characterized by high levels of H2-K1, ß4 integrin, and CD200 were described (Kathiriya et al., 2020). The LNEPs correspond to a small, quiescent subpopulation of Sca1-expressing, Scgb1a1-traced stem/progenitor cells without mature protein lineage markers and distinct from either *P63*+ basal cells or BASCs. Following bleomycin injury in vivo, these cells proliferate and differentiate into alveolar lineages. Our LTS-B cells, being lineage-traced by the *Sftpc*CreERT2 driver, are therefore right away distinct from LNEPs. We also checked by FACS, the expression of CD200, and found it to be expressed at a low level in LTS-B cells compared to LTS-A cells (data not shown).

Moreover, club cells in the conducting airway are reported to dedifferentiate into a basal stem cell population that can then expand and differentiate into several mature cell types, raising the possibility that club cell dedifferentiation is a pathway of regeneration in the injured lung (McQualter, 2019; Tata et al., 2013). Our scRNA-seq results on LTS-B show that these cells are distinct from club cells (Figure 6). In

addition, the expression of Scgb1a1 at the protein level was not significantly detected in LTS-B (Figure 7).

Interestingly, using transgenic mice with the human *SFTPC* promoter driving GFP expression (Chen et al., 2012), two populations of bronchial epithelial cells were identified based on the level of GFP expression. GFP^{low} was detected in the mid-level bronchioles, while GFP^{high} was found in terminal bronchioles and alveolar regions. Further characterization using Cd24 allowed separation of the $GFP^{high}CD24^{low}$ (GFP^{high} cells in the bronchi) from $GFP^{high}Cd24^{high}$ (GFP^{high} cells in the alveoli, aka AT2s). After bleomycin lung injury, only the $GFP^{high}CD24^{low}$ exhibited a strong expansion response during tissue remodeling, suggesting a crucial role in epithelial repair under injury conditions. Whether the $GFP^{high}CD24^{low}$ corresponds to the LTS-B remains unclear. Based on a close examination of gene expression differences between $GFP^{high}Cd24^{high}$ and AT2s (Chen et al., 2012)and between LTS-B and LTS-A cells (Aka AT2s, this study), our results suggest that LTS-B cells are still different from $GFP^{high}Cd24^{high}$. For example, genes such as *Sult1d1, Lypd2*, whose expression was not drastically different between $GFP^{high}Cd24^{high}$ and AT2s (Chen et al., 2012), are differentially expressed between LTS-B and LTS-A (own data, Supp Figure 17). We also found *Slc23a1, Pard6g,* and Ces1g, which are differentially expressed between GFP^{high}Cd24high and AT2s, are expressed at similar levels between LTS-B and LTS-A.

5.3 Towards the identification of human LTS-B-like cells

SFTPC+ cells have not been identified so far in the human lung bronchi. Interestingly, our data indicate that immature AT2-like cells negative for Sftpc protein and Lyzotracker staining, which are fundamentally different from the bona fide AT2 in the alveoli, exist in the bronchi in mice. Our study indicates that LTS-B acquires a *Krt8+Krt18+* ADI status upon injury. The acquisition of ADI-like characteristics, KRT5-negative/KRT17-positive (*KRT5−/KRT17+)* by the pulmonary epithelium in humans has been reported (Habermann et al., 2020). What is unclear, however, is whether these human cells originate from the alveolar and/or the bronchiolar compartment.

An important anatomical difference between the mouse and human conducting airways is the unique presence of the respiratory bronchioles in the human lung. These

respiratory bronchioles bridge the terminal bronchioles with the alveolar ducts and contain respiratory airway secretory (RAS) cells, which have been proposed to be essential for airway repair and regeneration. Indeed, RAS cells can act as progenitors for alveolar type 2 cells (Basil et al., 2022), providing a human context for airway-to-alveoli regeneration and showing that LTS-B cells in mice, which are enriched in the terminal bronchioles upon injury, could have a functional counterpart in human lungs. Interestingly, in the human lung, alveolar type 0 (AT0) cells have recently been identified as a transitional progenitor population in the distal airways. Murthy and colleagues characterized AT0 cells by their mixed molecular identity, as they co-express AT2 markers (e.g., *SFTPC*) along with alveolar type I (e.g., *AGER*) and secretory cell markers (e.g., *SCGB3A2*) – placing them at an intermediate state between AT2, AT1, and bronchiolar secretory cells (Kadur Lakshminarasimha Murthy et al., 2022). Functionally, AT0 cells appear to originate from AT2 cells and are bi-potent, capable of differentiating into gas-exchanging AT1 cells or into secretory epithelial cells of the terminal bronchiole, thus serving as progenitors at the alveolar–airway interface (Han et al., 2023). In parallel, our findings in the mouse lung reveal a conceptually similar progenitor cell reservoir in the airway. LTS-B cells, which also express Scgb3a2 (Figure 5J), reside in the bronchi but retain an alveolar lineage identity. Upon lung injury, these LTS-B cells become activated, markedly expand, and migrate out of the bronchi and enter an intermediate transitional state on the path toward alveolar differentiation. Moreover, under pro-differentiation conditions in vitro, LTS-B progenitors can partially acquire *Sftpc*GFP expression, highlighting their differentiation potential into alveolar cells. Together, the identification of LTS-B in mice alongside the AT0 population in humans suggests a conserved paradigm of regionally localized, hybrid-identity progenitors in the lung. This comparison underscores the novelty and significance of LTS-B as a previously unrecognized progenitor pool in the bronchi in mice that can bridge airway and alveolar lineages, contributing to alveolar regeneration in a manner complementary to the AT0 cells described in human lungs. Whether the mouse LTS-B are the human equivalent of the AT0 remains to be clarified using Dre/Cre intersectional genetics. Interestingly, from the stem cell point of view, mice and humans are not so different, in spite of anatomical differences regarding the exclusive presence of the respiratory bronchioles in humans.

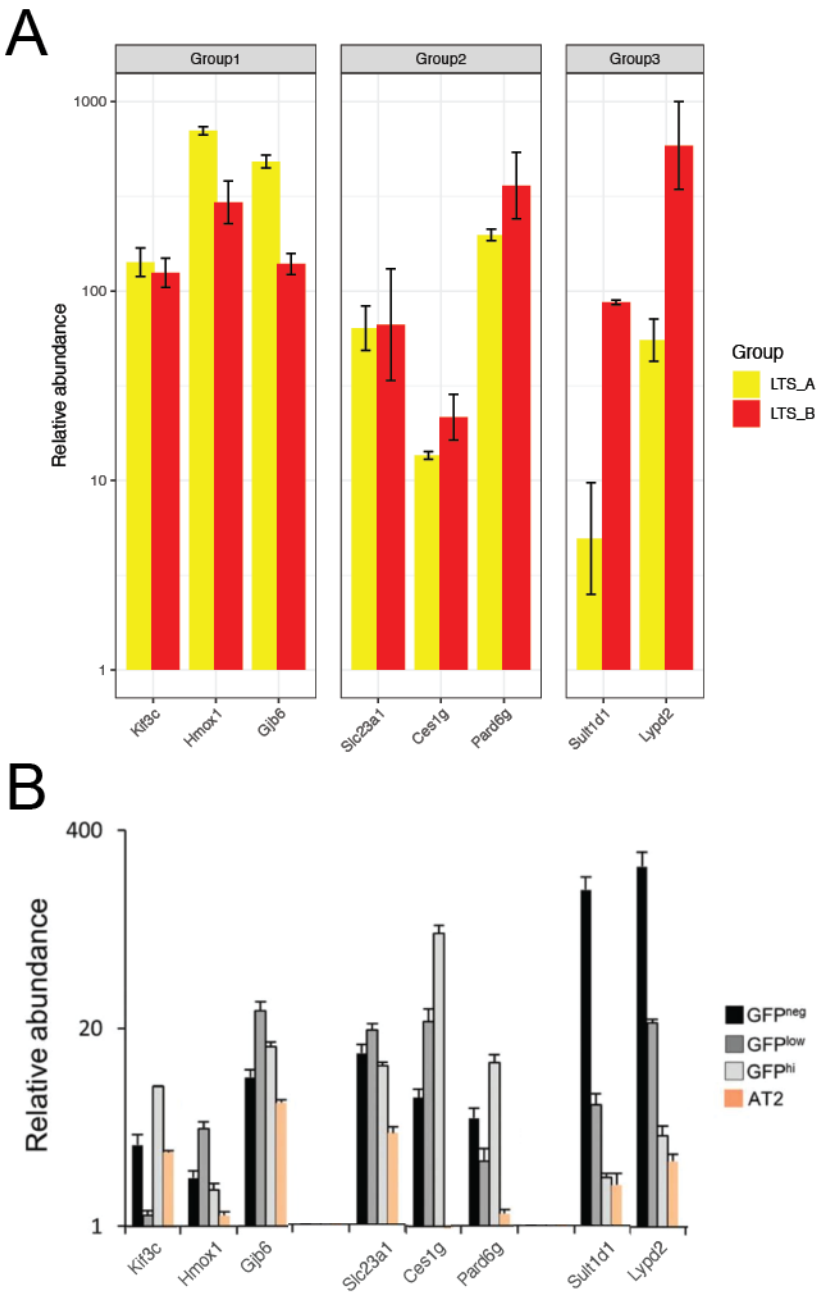

Figure 17: LTS-B cells are different from GFP^{high}Cd24^{high}.
A) The expression of three groups of genes selected based on the data from Chen et al (2012) comparing GFP^{high}Cd24^{high} versus AT2s are shown (please note that the expression of these genes shown in B is adapted from Chen et al., 2012). Group 1 and 2 genes are expressed at a higher level in GFP^{high}Cd24^{high} versus AT2s. These genes are expressed at a similar or at a lower level in LTS-B vs LTS-A. Group 3 genes are also expressed at a similar level in GFP^{high}Cd24^{high} versus AT2s, but are expressed at a higher level in LTS-B vs LTS-A.

Chapter 6: Summary

This dissertation investigates a novel progenitor population in the lung that was identified through *Sftpc* lineage-tracing experiments. This population resides in the bronchi and is distinct from classical AT2 cells. Although AT2 cells have long been considered the primary source of alveolar regeneration, lineage-tracing studies using *Sftpc*CreERT2 mice combined with Tomatoflox and *Sftpc*GFP reporters revealed an additional population of $tdTom^+$ GFP^- cells localized to the bronchial epithelium. This population is termed Lineage-Traced *Sftpc* Cells in the Bronchi (LTS-B). These cells represent approximately 1.6% of epithelial cells and occupy a unique niche on the apical side of bronchial smooth muscle. Interestingly, transcriptomic analysis revealed a hybrid identity with reduced AT2 signatures, enrichment of ciliated and club cell markers, activation of PI3K/Akt signaling, and reduced Fgfr2b signaling. These findings establish LTS-Bs as a distinct progenitor pool. Further analysis using single-cell RNA sequencing revealed heterogeneity within this population and identified two distinct subtypes of LTS-B based on transcription.

One cluster expresses *FoxJ1*, *Tpp3*, and markers, resembling ciliated cells. The other cluster expresses *Sftpc* and *Abca3*, resembling alveolar cells. This dual identity underscores their transitional nature, linking airway- and alveolar-like fates.

To study epithelial injury and repair dynamics, precision-cut lung slices (PCLS) were used in conjunction with in vivo naphthalene-induced injury. The PCLS model reproduced hallmarks of acute epithelial stress, including rapid declines in *Sftpc*, Epcam, and Scgb1a1 expression. This is followed by a partial recovery of mesenchymal and growth factor markers, such as *Fgf10* and *Acta2*. This reflects the initiation of repair programs. These results validate PCLS as a powerful ex vivo system for studying progenitor cell behavior. In this context, LTS-B cells expanded in response to injury, both in vivo and ex vivo. Live imaging revealed their motility and migration from the bronchi toward the alveolar area. Next, transcriptomic profiling revealed that LTS-B cells, upon 8 days of PCLS culture, adopt an alveolar differentiation intermediate (ADI)-like state, positioning them as transitional progenitors.

Treating PCLS with FGF10 and CHIR99021 partially induced LTS-B differentiation into *Sftpc*GFP^+ cells, suggesting their potential to contribute to alveolar lineages.

Comparative analyses revealed that LTS-Bs are distinct from other progenitor pools, including bronchioalveolar stem cells (BASCs), lineage-negative epithelial progenitors (LNEPs), and basal or club cell populations. Instead of being a variant of these cells, LTS-Bs constitute an unrecognized progenitor pool with a unique identity, localization, and behavior. Preliminary evidence from human idiopathic pulmonary fibrosis (IPF) samples suggests that LTS-B-like cells may exist in humans as well, sharing transcriptional features with the murine population. These findings raise the possibility that LTS-Bs participate in both physiological regeneration and maladaptive remodeling during chronic lung disease.

In summary, this dissertation identifies and characterizes LTS-B as a rare, bronchi-localized progenitor population that expands during injury and adopts an ADI-like transitional state. Under regenerative cues, this population can partially differentiate toward AT2 fate. Through the establishment of PCLS as a robust ex vivo injury model and the integration of transcriptomic approaches with functional assays, this study broadens our comprehension of epithelial plasticity in the lung and challenges the prevailing notion that AT2 cells are the sole facilitators of alveolar repair. The discovery of LTS-B highlights the complexity of progenitor hierarchies in the lung and opens new avenues for regenerative strategies. If equivalent cells exist in humans, they could be promising therapeutic targets for diseases such as IPF, COPD, and ARDS. However, dysregulated activation of these progenitors could contribute to pathological fibrosis. By identifying LTS-B, this dissertation provides a framework for rethinking epithelial regeneration and emphasizes the importance of exploring diverse progenitor pools in lung biology and disease.

Chapter 7: Zusammenfassung

Diese Dissertation untersucht eine neuartige Vorläuferpopulation in der Lunge, die durch *Sftpc*-Linienverfolgungsexperimente identifiziert wurde. Diese Population befindet sich in den Bronchien und unterscheidet sich von klassischen AT2-Zellen. Obwohl AT2-Zellen lange Zeit als primäre Quelle für die Alveolarregeneration galten, zeigten Abstammungsuntersuchungen mit *Sftpc*CreERT2-Mäusen in Kombination mit Tomatoflox- und *Sftpc*GFP-Reportern eine zusätzliche Population von $tdTom^{+}GFP^{-}$-Zellen, die im Bronchialepithel lokalisiert sind. Diese Population wird als Lineage-Traced *Sftpc* Cells in the Bronchi (LTS-B) bezeichnet. Diese Zellen machen etwa 1,6 % der Epithelzellen aus und besetzen eine einzigartige Nische auf der apikalen Seite der glatten Bronchialmuskulatur. Interessanterweise ergab die Transkriptomanalyse eine hybride Identität mit reduzierten AT2-Signaturen, einer Anreicherung von Markern für Flimmer- und Keulenzellen, einer Aktivierung der PI3K/Akt-Signalübertragung und einer reduzierten Fgfr2b-Signalübertragung. Diese Ergebnisse etablieren LTS-Bs als einen eigenständigen Vorläuferpool. Eine weitere Analyse mittels Einzelzell-RNA-Sequenzierung ergab eine Heterogenität innerhalb dieser Population und identifizierte zwei unterschiedliche Subtypen von LTS-B auf der Grundlage der Transkription.

Ein Cluster exprimiert *FoxJ1*- und *Tpp3*-Marker, die den Flimmerzellen ähneln. Die anderen Cluster exprimiert *Sftpc* und *Abca3*, die den Alveolarzellen ähneln. Diese doppelte Identität unterstreicht ihre Übergangsnatur, die Atemwegs- und Alveolar-ähnliche Schicksale miteinander verbindet.

Um die Dynamik von Epithelverletzungen und -reparaturen zu untersuchen, wurden präzisionsgeschnittene Lungenschnitte (PCLS) in Verbindung mit in vivo durch Naphthalin induzierten Verletzungen verwendet. Das PCLS-Modell reproduzierte die Kennzeichen akuter Epithelstress, darunter einen raschen Rückgang der Expression von *Sftpc*, *Epcam* und *Scgb1a1*. Darauf folgte eine teilweise Erholung der mesenchymalen und Wachstumsfaktor-Marker wie Fgf10 und Acta2. Dies spiegelt den Beginn von Reparaturprogrammen wider. Diese Ergebnisse bestätigen PCLS als leistungsfähiges Ex-vivo-System zur Untersuchung des Verhaltens von Vorläuferzellen. In diesem Zusammenhang vermehrten sich LTS-B-Zellen sowohl in vivo als auch ex vivo als Reaktion auf die Verletzung. Live-Bildgebung zeigte ihre Motilität und Migration von den Bronchien zum Alveolarbereich. Als Nächstes zeigte

die Transkriptom-Profilierung, dass LTS-B-Zellen nach 8 Tagen PCLS-Kultur einen ADI-ähnlichen (Alveolar Differentiation Intermediate) Zustand annehmen, wodurch sie als Übergangsvorläufer positioniert werden.
Die Behandlung von PCLS mit FGF10 und CHIR99021 induzierte teilweise die Differenzierung von LTS-B-Zellen zu *Sftpc*GFP$^+$-Zellen, was auf ihr Potenzial hinweist, zu alveolären Linien beizutragen.
Vergleichende Analysen ergaben, dass sich LTS-Bs von anderen Vorläuferzellpools unterscheiden, darunter bronchioalveoläre Stammzellen (BASCs), liniennegative epitheliale Vorläuferzellen (LNEPs) und basale oder Clubzellpopulationen. Anstatt eine Variante dieser Zellen zu sein, bilden LTS-Bs einen bisher unbekannten Vorläuferzellpool mit einer einzigartigen Identität, Lokalisierung und Verhaltensweise. Vorläufige Erkenntnisse aus Proben von Patienten mit idiopathischer Lungenfibrose (IPF) deuten darauf hin, dass LTSB-ähnliche Zellen auch beim Menschen vorkommen und transkriptionelle Merkmale mit der murinen Population teilen. Diese Ergebnisse lassen vermuten, dass LTSBs sowohl an der physiologischen Regeneration als auch an der maladaptiven Umgestaltung bei chronischen Lungenerkrankungen beteiligt sind.
Zusammenfassend identifiziert und charakterisiert diese Dissertation LTS-B als eine seltene, in den Bronchien lokalisierte Vorläuferpopulation, die sich während einer Verletzung ausdehnt und einen ADI-ähnlichen Übergangszustand annimmt. Unter regenerativen Signalen kann sich diese Population teilweise in Richtung AT2 differenzieren. Durch die Etablierung von PCLS als robustes Ex-vivo-Verletzungsmodell und die Integration von transkriptomischen Ansätzen mit funktionellen Assays erweitert diese Studie unser Verständnis der epithelialen Plastizität in der Lunge und stellt die vorherrschende Vorstellung in Frage, dass AT2-Zellen die einzigen Vermittler der Alveolarreparatur sind. Die Entdeckung von LTS-B unterstreicht die Komplexität der Vorläuferzellhierarchien in der Lunge und eröffnet neue Wege für regenerative Strategien. Wenn es beim Menschen gleichwertige Zellen gibt, könnten sie vielversprechende therapeutische Ziele für Krankheiten wie IPF, COPD und ARDS sein. Eine dysregulierte Aktivierung dieser Vorläuferzellen könnte jedoch zu pathologischer Fibrose beitragen. Durch die Identifizierung von LTS-B liefert diese Dissertation einen Rahmen für ein neues Verständnis der epithelialen

Regeneration und betont die Bedeutung der Erforschung verschiedener Vorläuferzellpools in der Lungenbiologie und bei Lungenerkrankungen.

Chapter 8: References

Ahmadvand, N., Khosravi, F., Lingampally, A., Wasnick, R., Vazquez-Armendariz, A. I., Carraro, G., Heiner, M., Rivetti, S., Lv, Y., Wilhelm, J., Gunther, A., Herold, S., Al Alam, D., Chen, C., Minoo, P., Zhang, J.-S., & Bellusci, S. (2021). Identification of a novel subset of alveolar type 2 cells enriched in PD-L1 and expanded following pneumonectomy. *European Respiratory Journal*, *58*(5), 2004168. https://doi.org/10.1183/13993003.04168-2020

Alsafadi, H. N., Uhl, F. E., Pineda, R. H., Bailey, K. E., Rojas, M., Wagner, D. E., & Königshoff, M. (2020). Applications and Approaches for Three-Dimensional Precision-Cut Lung Slices. Disease Modeling and Drug Discovery. *American Journal of Respiratory Cell and Molecular Biology*, *62*(6), 681–691. https://doi.org/10.1165/rcmb.2019-0276TR

Alysandratos, K.-D., Garcia-de-Alba, C., Yao, C., Pessina, P., Huang, J., Villacorta-Martin, C., Hix, O. T., Minakin, K., Burgess, C. L., Bawa, P., Murthy, A., Konda, B., Beers, M. F., Stripp, B. R., Kim, C. F., & Kotton, D. N. (2023). Culture impact on the transcriptomic programs of primary and iPSC-derived human alveolar type 2 cells. *JCI Insight*, *8*(1). https://doi.org/10.1172/jci.insight.158937

Aoshiba, K., Tsuji, T., Itoh, M., Semba, S., Yamaguchi, K., Nakamura, H., & Watanabe, H. (2014). A murine model of airway fibrosis induced by repeated naphthalene exposure. *Experimental and Toxicologic Pathology*, *66*(4), 169–177. https://doi.org/10.1016/j.etp.2014.01.001

Barkauskas, C. E., Cronce, M. J., Rackley, C. R., Bowie, E. J., Keene, D. R., Stripp, B. R., Randell, S. H., Noble, P. W., & Hogan, B. L. M. (2013). Type 2 alveolar cells are stem cells in adult lung. *Journal of Clinical Investigation*, *123*(7), 3025–3036. https://doi.org/10.1172/JCI68782

Barreiro Carpio, M., Dabaghi, M., Ungureanu, J., Kolb, M. R., Hirota, J. A., & Moran-Mirabal, J. M. (2021). 3D Bioprinting Strategies, Challenges, and Opportunities to Model the Lung Tissue Microenvironment and Its Function.

Frontiers in Bioengineering and Biotechnology, *9*. https://doi.org/10.3389/fbioe.2021.773511

Basil, M. C., Alysandratos, K.-D., Kotton, D. N., & Morrisey, E. E. (2024). Lung repair and regeneration: Advanced models and insights into human disease. *Cell Stem Cell*, *31*(4), 439–454. https://doi.org/10.1016/j.stem.2024.02.009

Basil, M. C., Cardenas-Diaz, F. L., Kathiriya, J. J., Morley, M. P., Carl, J., Brumwell, A. N., Katzen, J., Slovik, K. J., Babu, A., Zhou, S., Kremp, M. M., McCauley, K. B., Li, S., Planer, J. D., Hussain, S. S., Liu, X., Windmueller, R., Ying, Y., Stewart, K. M., … Morrisey, E. E. (2022). Human distal airways contain a multipotent secretory cell that can regenerate alveoli. *Nature*, *604*(7904), 120–126. https://doi.org/10.1038/s41586-022-04552-0

Battaglini, D., Fazzini, B., Silva, P. L., Cruz, F. F., Ball, L., Robba, C., Rocco, P. R. M., & Pelosi, P. (2023). Challenges in ARDS Definition, Management, and Identification of Effective Personalized Therapies. *Journal of Clinical Medicine*, *12*(4), 1381. https://doi.org/10.3390/jcm12041381

Chao, C.-M., Moiseenko, A., Zimmer, K.-P., & Bellusci, S. (2016). Alveologenesis: key cellular players and fibroblast growth factor 10 signaling. *Molecular and Cellular Pediatrics*, *3*, 17. https://doi.org/10.1186/s40348-016-0045-7

Chapman, H. A., Li, X., Alexander, J. P., Brumwell, A., Lorizio, W., Tan, K., Sonnenberg, A., Wei, Y., & Vu, T. H. (2011). Integrin α6β4 identifies an adult distal lung epithelial population with regenerative potential in mice. *Journal of Clinical Investigation*, *121*(7), 2855–2862. https://doi.org/10.1172/JCI57673

Chen, H., Matsumoto, K., Brockway, B. L., Rackley, C. R., Liang, J., Lee, J.-H., Jiang, D., Noble, P. W., Randell, S. H., Kim, C. F., & Stripp, B. R. (2012). Airway Epithelial Progenitors Are Region Specific and Show Differential Responses to Bleomycin-Induced Lung Injury. *Stem Cells*, *30*(9), 1948–1960. https://doi.org/10.1002/stem.1150

Chioccioli, M., Liu, S., Magruder, S., Tata, A., Borriello, L., McDonough, J. E., Konkimalla, A., Kim, S.-H., Nouws, J., Gonzalez, D. G., Traub, B., Ye, X., Yang, T., Entenberg, D. R., Krishnaswamy, S., Hendry, C. E., Kaminski, N., Tata, P. R., & Sauler, M. (2024). Stem cell migration drives lung repair in

living mice. *Developmental Cell*, *59*(7), 830-840.e4. https://doi.org/10.1016/j.devcel.2024.02.003

Choi, J., Park, J.-E., Tsagkogeorga, G., Yanagita, M., Koo, B.-K., Han, N., & Lee, J.-H. (2020). Inflammatory Signals Induce AT2 Cell-Derived Damage-Associated Transient Progenitors that Mediate Alveolar Regeneration. *Cell Stem Cell*, *27*(3), 366-382.e7. https://doi.org/10.1016/j.stem.2020.06.020

Chong, L., Ahmadvand, N., Noori, A., Lv, Y., Chen, C., Bellusci, S., & Zhang, J.-S. (2023). Injury activated alveolar progenitors (IAAPs): the underdog of lung repair. *Cellular and Molecular Life Sciences*, *80*(6), 145. https://doi.org/10.1007/s00018-023-04789-6

Clevers, H. (2016). Modeling Development and Disease with Organoids. *Cell*, *165*(7), 1586–1597. https://doi.org/10.1016/j.cell.2016.05.082

Crosby, L. M., & Waters, C. M. (2010). Epithelial repair mechanisms in the lung. *American Journal of Physiology-Lung Cellular and Molecular Physiology*, *298*(6), L715–L731. https://doi.org/10.1152/ajplung.00361.2009

El Agha, E., & Thannickal, V. J. (2023). The lung mesenchyme in development, regeneration, and fibrosis. *Journal of Clinical Investigation*, *133*(14). https://doi.org/10.1172/JCI170498

Evans, M. J., Cabral, L. J., Stephens, R. J., & Freeman, G. (1975). Transformation of alveolar Type 2 cells to Type 1 cells following exposure to NO2. *Experimental and Molecular Pathology*, *22*(1), 142–150. https://doi.org/10.1016/0014-4800(75)90059-3

Evans, K. V., & Lee, J.-H. (2020). Alveolar wars: The rise of in vitro models to understand human lung alveolar maintenance, regeneration, and disease. *Stem Cells Translational Medicine*, *9*(8), 867–881. https://doi.org/10.1002/sctm.19-0433

Franks, T. J., Colby, T. V., Travis, W. D., Tuder, R. M., Reynolds, H. Y., Brody, A. R., Cardoso, W. V., Crystal, R. G., Drake, C. J., Engelhardt, J., Frid, M., Herzog, E., Mason, R., Phan, S. H., Randell, S. H., Rose, M. C., Stevens, T., Serge, J., Sunday, M. E., … Williams, M. C. (2008). Resident Cellular Components of the Human Lung: Current Knowledge and Goals for Research on Cell Phenotyping and Function. *Proceedings of the American*

Thoracic Society, *5*(7), 763–766. https://doi.org/10.1513/pats.200803-025HR

Gotoh, S., Ito, I., Nagasaki, T., Yamamoto, Y., Konishi, S., Korogi, Y., Matsumoto, H., Muro, S., Hirai, T., Funato, M., Mae, S.-I., Toyoda, T., Sato-Otsubo, A., Ogawa, S., Osafune, K., & Mishima, M. (2014). Generation of Alveolar Epithelial Spheroids via Isolated Progenitor Cells from Human Pluripotent Stem Cells. *Stem Cell Reports*, *3*(3), 394–403. https://doi.org/10.1016/j.stemcr.2014.07.005

Habermann, A. C., Gutierrez, A. J., Bui, L. T., Yahn, S. L., Winters, N. I., Calvi, C. L., Peter, L., Chung, M.-I., Taylor, C. J., Jetter, C., Raju, L., Roberson, J., Ding, G., Wood, L., Sucre, J. M. S., Richmond, B. W., Serezani, A. P., McDonnell, W. J., Mallal, S. B., … Kropski, J. A. (2020). Single-cell RNA sequencing reveals profibrotic roles of distinct epithelial and mesenchymal lineages in pulmonary fibrosis. *Science Advances*, *6*(28). https://doi.org/10.1126/sciadv.aba1972

Han, S., Budinger, G. R. S., & Gottardi, C. J. (2023). Alveolar epithelial regeneration in the aging lung. *Journal of Clinical Investigation*, *133*(20). https://doi.org/10.1172/JCI170504

Hao, Y., Stuart, T., Kowalski, M. H., Choudhary, S., Hoffman, P., Hartman, A., Srivastava, A., Molla, G., Madad, S., Fernandez-Granda, C., & Satija, R. (2024). Dictionary learning for integrative, multimodal and scalable single-cell analysis. *Nature Biotechnology*, *42*(2), 293–304. https://doi.org/10.1038/s41587-023-01767-y

Hawkins, F. J., Suzuki, S., Beermann, M. Lou, Barillà, C., Wang, R., Villacorta-Martin, C., Berical, A., Jean, J. C., Le Suer, J., Matte, T., Simone-Roach, C., Tang, Y., Schlaeger, T. M., Crane, A. M., Matthias, N., Huang, S. X. L., Randell, S. H., Wu, J., Spence, J. R., … Kotton, D. N. (2021). Derivation of Airway Basal Stem Cells from Human Pluripotent Stem Cells. *Cell Stem Cell*, *28*(1), 79-95.e8. https://doi.org/10.1016/j.stem.2020.09.017

Hawkins, F., Kramer, P., Jacob, A., Driver, I., Thomas, D. C., McCauley, K. B., Skvir, N., Crane, A. M., Kurmann, A. A., Hollenberg, A. N., Nguyen, S., Wong, B. G., Khalil, A. S., Huang, S. X. L., Guttentag, S., Rock, J. R., Shannon, J. M., Davis, B. R., & Kotton, D. N. (2017). Prospective isolation

of NKX2-1–expressing human lung progenitors derived from pluripotent stem cells. *Journal of Clinical Investigation*, *127*(6), 2277–2294. https://doi.org/10.1172/JCI89950

Huang, S. X. L., Green, M. D., de Carvalho, A. T., Mumau, M., Chen, Y.-W., D'Souza, S. L., & Snoeck, H.-W. (2015). The in vitro generation of lung and airway progenitor cells from human pluripotent stem cells. *Nature Protocols*, *10*(3), 413–425. https://doi.org/10.1038/nprot.2015.023

Jacob, A., Morley, M., Hawkins, F., McCauley, K. B., Jean, J. C., Heins, H., Na, C.-L., Weaver, T. E., Vedaie, M., Hurley, K., Hinds, A., Russo, S. J., Kook, S., Zacharias, W., Ochs, M., Traber, K., Quinton, L. J., Crane, A., Davis, B. R., … Kotton, D. N. (2017). Differentiation of Human Pluripotent Stem Cells into Functional Lung Alveolar Epithelial Cells. *Cell Stem Cell*, *21*(4), 472-488.e10. https://doi.org/10.1016/j.stem.2017.08.014

Jain, R., Barkauskas, C. E., Takeda, N., Bowie, E. J., Aghajanian, H., Wang, Q., Padmanabhan, A., Manderfield, L. J., Gupta, M., Li, D., & others. (2015). Plasticity of Hopx(+) type I alveolar cells to regenerate type II cells in the lung. *Nature Communications*, *6*, 6727. https://doi.org/10.1038/ncomms7727

Jakwerth, C. A., Ordovas-Montanes, J., Blank, S., Schmidt-Weber, C. B., & Zissler, U. M. (2022). Role of Respiratory Epithelial Cells in Allergic Diseases. *Cells*, *11*(9), 1387. https://doi.org/10.3390/cells11091387

Jansing, N. L., McClendon, J., Henson, P. M., Tuder, R. M., Hyde, D. M., & Zemans, R. L. (2017). Unbiased Quantitation of Alveolar Type II to Alveolar Type I Cell Transdifferentiation during Repair after Lung Injury in Mice. *American Journal of Respiratory Cell and Molecular Biology*, *57*(5), 519–526. https://doi.org/10.1165/rcmb.2017-0037MA

Jiang, M., Roth, M. G., Chun-on, P., Sullivan, D. I., & Alder, J. K. (2020). Phenotypic Diversity Caused by Differential Expression of *SFTPC* -Cre–Transgenic Alleles. *American Journal of Respiratory Cell and Molecular Biology*, *62*(6), 692–698. https://doi.org/10.1165/rcmb.2019-0416MA

Jurado, M. R., Tombor, L. S., Arsalan, M., Holubec, T., Emrich, F., Walther, T., Abplanalp, W., Fischer, A., Zeiher, A. M., Schulz, M. H., Dimmeler, S., & John, D. (2024). Improved integration of single-cell transcriptome data

demonstrates common and unique signatures of heart failure in mice and humans. *GigaScience*, *13*. https://doi.org/10.1093/gigascience/giae011

Kadur Lakshminarasimha Murthy, P., Sontake, V., Tata, A., Kobayashi, Y., Macadlo, L., Okuda, K., Conchola, A. S., Nakano, S., Gregory, S., Miller, L. A., Spence, J. R., Engelhardt, J. F., Boucher, R. C., Rock, J. R., Randell, S. H., & Tata, P. R. (2022). Human distal lung maps and lineage hierarchies reveal a bipotent progenitor. *Nature*, *604*(7904), 111–119. https://doi.org/10.1038/s41586-022-04541-3

Kathiriya, J. J., Brumwell, A. N., Jackson, J. R., Tang, X., & Chapman, H. A. (2020). Distinct Airway Epithelial Stem Cells Hide among Club Cells but Mobilize to Promote Alveolar Regeneration. *Cell Stem Cell*, *26*(3), 346-358.e4. https://doi.org/10.1016/j.stem.2019.12.014

Kim, C. F. B., Jackson, E. L., Woolfenden, A. E., Lawrence, S., Babar, I., Vogel, S., Crowley, D., Bronson, R. T., & Jacks, T. (2005). Identification of Bronchioalveolar Stem Cells in Normal Lung and Lung Cancer. *Cell*, *121*(6), 823–835. https://doi.org/10.1016/j.cell.2005.03.032

Kobayashi, Y., Tata, A., Konkimalla, A., Katsura, H., Lee, R. F., Ou, J., Banovich, N. E., Kropski, J. A., & Tata, P. R. (2020). Persistence of a regeneration-associated, transitional alveolar epithelial cell state in pulmonary fibrosis. *Nature Cell Biology*, *22*(8), 934–946. https://doi.org/10.1038/s41556-020-0542-8

Korsunsky, I., Millard, N., Fan, J., Slowikowski, K., Zhang, F., Wei, K., Baglaenko, Y., Brenner, M., Loh, P., & Raychaudhuri, S. (2019). Fast, sensitive and accurate integration of single-cell data with Harmony. *Nature Methods*, *16*(12), 1289–1296. https://doi.org/10.1038/s41592-019-0619-0

Kotton, D. N., & Morrisey, E. E. (2014). Lung regeneration: mechanisms, applications and emerging stem cell populations. *Nature Medicine*, *20*(8), 822–832. https://doi.org/10.1038/nm.3642

Koziol-White, C., Gebski, E., Cao, G., & Panettieri, R. A. (2024). Precision cut lung slices: an integrated ex vivo model for studying lung physiology, pharmacology, disease pathogenesis and drug discovery. *Respiratory Research*, *25*(1), 231. https://doi.org/10.1186/s12931-024-02855-6

Kumar, P. A., Hu, Y., Yamamoto, Y., Hoe, N. B., Wei, T. S., Mu, D., Sun, Y., Joo, L. S., Dagher, R., Zielonka, E. M., Wang, D. Y., Lim, B., Chow, V. T., Crum, C. P., Xian, W., & McKeon, F. (2011). Distal Airway Stem Cells Yield Alveoli In Vitro and during Lung Regeneration following H1N1 Influenza Infection. *Cell*, *147*(3), 525–538. https://doi.org/10.1016/j.cell.2011.10.001

Lee, J.-H., Kim, J., Gludish, D., Roach, R. R., Saunders, A. H., Barrios, J., Woo, A. J., Chen, H., Conner, D. A., Fujiwara, Y., Stripp, B. R., & Kim, C. F. (2013). Surfactant Protein–C Chromatin-Bound Green Fluorescence Protein Reporter Mice Reveal Heterogeneity of Surfactant Protein C–Expressing Lung Cells. *American Journal of Respiratory Cell and Molecular Biology*, *48*(3), 288–298. https://doi.org/10.1165/rcmb.2011-0403OC

Lehmann, M., Buhl, L., Alsafadi, H. N., Klee, S., Hermann, S., Mutze, K., Ota, C., Lindner, M., Behr, J., Hilgendorff, A., Wagner, D. E., & Königshoff, M. (2018). Differential effects of Nintedanib and Pirfenidone on lung alveolar epithelial cell function in ex vivo murine and human lung tissue cultures of pulmonary fibrosis. *Respiratory Research*, *19*(1), 175. https://doi.org/10.1186/s12931-018-0876-y

Liu, Q., Liu, K., Cui, G., Huang, X., Yao, S., Guo, W., Qin, Z., Li, Y., Yang, R., Pu, W., Zhang, L., He, L., Zhao, H., Yu, W., Tang, M., Tian, X., Cai, D., Nie, Y., Hu, S., … Zhou, B. (2019). Lung regeneration by multipotent stem cells residing at the bronchioalveolar-duct junction. *Nature Genetics*, *51*(4), 728–738. https://doi.org/10.1038/s41588-019-0346-6

Longmire, T. A., Ikonomou, L., Hawkins, F., Christodoulou, C., Cao, Y., Jean, J. C., Kwok, L. W., Mou, H., Rajagopal, J., Shen, S. S., Dowton, A. A., Serra, M., Weiss, D. J., Green, M. D., Snoeck, H.-W., Ramirez, M. I., & Kotton, D. N. (2012). Efficient Derivation of Purified Lung and Thyroid Progenitors from Embryonic Stem Cells. *Cell Stem Cell*, *10*(4), 398–411. https://doi.org/10.1016/j.stem.2012.01.019

Madisen, L., Zwingman, T. A., Sunkin, S. M., Oh, S. W., Zariwala, H. A., Gu, H., Ng, L. L., Palmiter, R. D., Hawrylycz, M. J., Jones, A. R., Lein, E. S., & Zeng, H. (2010). A robust and high-throughput Cre reporting and characterization system for the whole mouse brain. *Nature Neuroscience*, *13*(1), 133–140. https://doi.org/10.1038/nn.2467

McCauley, K. B., Alysandratos, K.-D., Jacob, A., Hawkins, F., Caballero, I. S., Vedaie, M., Yang, W., Slovik, K. J., Morley, M., Carraro, G., Kook, S., Guttentag, S. H., Stripp, B. R., Morrisey, E. E., & Kotton, D. N. (2018). Single-Cell Transcriptomic Profiling of Pluripotent Stem Cell-Derived SCGB3A2+ Airway Epithelium. *Stem Cell Reports*, *10*(5), 1579–1595. https://doi.org/10.1016/j.stemcr.2018.03.013

McCauley, K. B., Hawkins, F., Serra, M., Thomas, D. C., Jacob, A., & Kotton, D. N. (2017). Efficient Derivation of Functional Human Airway Epithelium from Pluripotent Stem Cells via Temporal Regulation of Wnt Signaling. *Cell Stem Cell*, *20*(6), 844-857.e6. https://doi.org/10.1016/j.stem.2017.03.001

McQualter, J. L. (2019). Endogenous lung stem cells for lung regeneration. *Expert Opinion on Biological Therapy*, *19*(6), 539–546. https://doi.org/10.1080/14712598.2019.1596256

McQualter, J. L., Yuen, K., Williams, B., & Bertoncello, I. (2010). Evidence of an epithelial stem/progenitor cell hierarchy in the adult mouse lung. *Proceedings of the National Academy of Sciences*, *107*(4), 1414–1419. https://doi.org/10.1073/pnas.0909207107

Mou, H., Zhao, R., Sherwood, R., Ahfeldt, T., Lapey, A., Wain, J., Sicilian, L., Izvolsky, K., Lau, F. H., Musunuru, K., Cowan, C., & Rajagopal, J. (2012). Generation of Multipotent Lung and Airway Progenitors from Mouse ESCs and Patient-Specific Cystic Fibrosis iPSCs. *Cell Stem Cell*, *10*(4), 385–397. https://doi.org/10.1016/j.stem.2012.01.018

Mulugeta, S., & Beers, M. F. (2006). Surfactant protein C: Its unique properties and emerging immunomodulatory role in the lung. *Microbes and Infection*, *8*(8), 2317–2323. https://doi.org/10.1016/j.micinf.2006.04.009

Nabhan, A. N., Brownfield, D. G., Harbury, P. B., Krasnow, M. A., & Desai, T. J. (2018). Single-cell Wnt signaling niches maintain stemness of alveolar type 2 cells. *Science*, *359*(6380), 1118–1123. https://doi.org/10.1126/science.aam6603

Narasaraju, T., Ng, H. H., Phoon, M. C., & Chow, V. T. K. (2010). MCP-1 Antibody Treatment Enhances Damage and Impedes Repair of the Alveolar Epithelium in Influenza Pneumonitis. *American Journal of Respiratory Cell*

and Molecular Biology, *42*(6), 732–743. https://doi.org/10.1165/rcmb.2008-0423OC

Negretti, N. M., Plosa, E. J., Benjamin, J. T., Schuler, B. A., Habermann, A. C., Jetter, C. S., Gulleman, P., Bunn, C., Hackett, A. N., Ransom, M., Taylor, C. J., Nichols, D., Matlock, B. K., Guttentag, S. H., Blackwell, T. S., Banovich, N. E., Kropski, J. A., & Sucre, J. M. S. (2021). A single-cell atlas of mouse lung development. *Development*, *148*(24). https://doi.org/10.1242/dev.199512

Otelea, M. R., Oancea, C., Reisz, D., Vaida, M. A., Maftei, A., & Popescu, F. G. (2023). Club Cells—A Guardian against Occupational Hazards. *Biomedicines*, *12*(1), 78. https://doi.org/10.3390/biomedicines12010078

Penkala, I. J., Liberti, D. C., Pankin, J., Sivakumar, A., Kremp, M. M., Jayachandran, S., Katzen, J., Leach, J. P., Windmueller, R., Stolz, K., & others. (2021). Age-dependent alveolar epithelial plasticity orchestrates lung homeostasis and regeneration. *Cell Stem Cell*, *28*, 1775-1789.e1775. https://doi.org/10.1016/j.stem.2021.04.026

Rawlins, E. L., & Perl, A.-K. (2012). The a“MAZE”ing World of Lung-Specific Transgenic Mice. *American Journal of Respiratory Cell and Molecular Biology*, *46*(3), 269–282. https://doi.org/10.1165/rcmb.2011-0372PS

Reddy, R., Buckley, S., Doerken, M., Barsky, L., Weinberg, K., Anderson, K. D., Warburton, D., & Driscoll, B. (2004). Isolation of a putative progenitor subpopulation of alveolar epithelial type 2 cells. *American Journal of Physiology-Lung Cellular and Molecular Physiology*, *286*(4), L658–L667. https://doi.org/10.1152/ajplung.00159.2003

Rock, J. R., Onaitis, M. W., Rawlins, E. L., Lu, Y., Clark, C. P., Xue, Y., Randell, S. H., & Hogan, B. L. M. (2009). Basal cells as stem cells of the mouse trachea and human airway epithelium. *Proceedings of the National Academy of Sciences*, *106*(31), 12771–12775. https://doi.org/10.1073/pnas.0906850106

Salwig, I., Spitznagel, B., Vazquez-Armendariz, A. I., Khalooghi, K., Guenther, S., Herold, S., Szibor, M., & Braun, T. (2019). Bronchioalveolar stem cells are a main source for regeneration of distal lung epithelia *in vivo*. *The EMBO Journal*, *38*(12). https://doi.org/10.15252/embj.2019102099

Sauer, B., & Henderson, N. (1988). Site-specific DNA recombination in mammalian cells by the Cre recombinase of bacteriophage P1. *Proceedings of the National Academy of Sciences*, *85*(14), 5166–5170. https://doi.org/10.1073/pnas.85.14.5166

Schindelin, J., Arganda-Carreras, I., Frise, E., Kaynig, V., Longair, M., Pietzsch, T., Preibisch, S., Rueden, C., Saalfeld, S., Schmid, B., Tinevez, J.-Y., White, D. J., Hartenstein, V., Eliceiri, K., Tomancak, P., & Cardona, A. (2012). Fiji: an open-source platform for biological-image analysis. *Nature Methods*, *9*(7), 676–682. https://doi.org/10.1038/nmeth.2019

Strunz, M., Simon, L. M., Ansari, M., Kathiriya, J. J., Angelidis, I., Mayr, C. H., Tsidiridis, G., Lange, M., Mattner, L. F., Yee, M., Ogar, P., Sengupta, A., Kukhtevich, I., Schneider, R., Zhao, Z., Voss, C., Stoeger, T., Neumann, J. H. L., Hilgendorff, A., … Schiller, H. B. (2020). Alveolar regeneration through a Krt8+ transitional stem cell state that persists in human lung fibrosis. *Nature Communications*, *11*(1), 3559. https://doi.org/10.1038/s41467-020-17358-3

Taghizadeh, S., Heiner, M., Vazquez-Armendariz, A. I., Wilhelm, J., Herold, S., Chen, C., Zhang, J. S., & Bellusci, S. (2021). Characterization in Mice of the Resident Mesenchymal Niche Maintaining At2 Stem Cell Proliferation in Homeostasis and Disease. *Stem Cells*, *39*(10), 1382–1394. https://doi.org/10.1002/stem.3423

Tata, P. R., Mou, H., Pardo-Saganta, A., Zhao, R., Prabhu, M., Law, B. M., Vinarsky, V., Cho, J. L., Breton, S., Sahay, A., Medoff, B. D., & Rajagopal, J. (2013). Dedifferentiation of committed epithelial cells into stem cells in vivo. *Nature*, *503*(7475), 218–223. https://doi.org/10.1038/nature12777

Tata, P. R., & Rajagopal, J. (2017). Plasticity in the lung: making and breaking cell identity. *Development*, *144*(5), 755–766. https://doi.org/10.1242/dev.143784

Vanderbilt, J. N., Gonzalez, R. F., Allen, L., Gillespie, A., Leaffer, D., Dean, W. B., Chapin, C., & Dobbs, L. G. (2015). High-Efficiency Type II Cell–Enhanced Green Fluorescent Protein Expression Facilitates Cellular Identification, Tracking, and Isolation. *American Journal of Respiratory Cell*

and Molecular Biology, *53*(1), 14–21. https://doi.org/10.1165/rcmb.2014-0348MA

Vaughan, A. E., Brumwell, A. N., Xi, Y., Gotts, J. E., Brownfield, D. G., Treutlein, B., Tan, K., Tan, V., Liu, F. C., Looney, M. R., Matthay, M. A., Rock, J. R., & Chapman, H. A. (2015a). Lineage-negative progenitors mobilize to regenerate lung epithelium after major injury. *Nature*, *517*(7536), 621–625. https://doi.org/10.1038/nature14112

Vaughan, A. E., Brumwell, A. N., Xi, Y., Gotts, J. E., Brownfield, D. G., Treutlein, B., Tan, K., Tan, V., Liu, F. C., Looney, M. R., Matthay, M. A., Rock, J. R., & Chapman, H. A. (2015b). Lineage-negative progenitors mobilize to regenerate lung epithelium after major injury. *Nature*, *517*(7536), 621–625. https://doi.org/10.1038/nature14112

Weibel, E. R., Sapoval, B., & Filoche, M. (2005). Design of peripheral airways for efficient gas exchange. *Respiratory Physiology & Neurobiology*, *148*(1–2), 3–21. https://doi.org/10.1016/j.resp.2005.03.005

Xu, H., Pan, G., & Wang, J. (2023). Repairing Mechanisms for Distal Airway Injuries and Related Targeted Therapeutics for Chronic Lung Diseases. *Cell Transplantation*, *32*. https://doi.org/10.1177/09636897231196489

Xu, J., Yu, H., & Sun, X. (2020). Less Is More: Rare Pulmonary Neuroendocrine Cells Function as Critical Sensors in Lung. *Developmental Cell*, *55*(2), 123–132. https://doi.org/10.1016/j.devcel.2020.09.024

Yaghi, A., & Dolovich, M. (2016). Airway Epithelial Cell Cilia and Obstructive Lung Disease. *Cells*, *5*(4), 40. https://doi.org/10.3390/cells5040040

Yee, M., Buczynski, B. W., & O'Reilly, M. A. (2014). Neonatal Hyperoxia Stimulates the Expansion of Alveolar Epithelial Type II Cells. *American Journal of Respiratory Cell and Molecular Biology*, *50*(4), 757–766. https://doi.org/10.1165/rcmb.2013-0207OC

Zacharias, W. J., Frank, D. B., Zepp, J. A., Morley, M. P., Alkhaleel, F. A., Kong, J., Zhou, S., Cantu, E., & Morrisey, E. E. (2018). Regeneration of the lung alveolus by an evolutionarily conserved epithelial progenitor. *Nature*, *555*(7695), 251–255. https://doi.org/10.1038/nature25786

Zamprogno, P., Wüthrich, S., Achenbach, S., Thoma, G., Stucki, J. D., Hobi, N., Schneider-Daum, N., Lehr, C.-M., Huwer, H., Geiser, T., Schmid, R. A., &

Guenat, O. T. (2021). Second-generation lung-on-a-chip with an array of stretchable alveoli made with a biological membrane. *Communications Biology*, *4*(1), 168. https://doi.org/10.1038/s42003-021-01695-0

Zheng, D., Limmon, G. V., Yin, L., Leung, N. H. N., Yu, H., Chow, V. T. K., & Chen, J. (2012). Regeneration of Alveolar Type I and II Cells from Scgb1a1-Expressing Cells following Severe Pulmonary Damage Induced by Bleomycin and Influenza. *PLoS ONE*, *7*(10), e48451. https://doi.org/10.1371/journal.pone.0048451

Zou, J., Sun, T., Song, X., Liu, Y.-M., Lei, F., Chen, M.-M., Chen, Z., Zhang, P., Ji, Y.-X., Zhang, X.-J., She, Z.-G., Cai, J., Luo, Y., Wang, P., & Li, H. (2022). Distributions and trends of the global burden of COPD attributable to risk factors by SDI, age, and sex from 1990 to 2019: a systematic analysis of GBD 2019 data. *Respiratory Research*, *23*(1), 90. https://doi.org/10.1186/s12931-022-02011-y

Zuo, W., Zhang, T., Wu, D. Z., Guan, S. P., Liew, A.-A., Yamamoto, Y., Wang, X., Lim, S. J., Vincent, M., Lessard, M., Crum, C. P., Xian, W., & McKeon, F. (2015). p63+Krt5+ distal airway stem cells are essential for lung regeneration. *Nature*, *517*(7536), 616–620. https://doi.org/10.1038/nature13903

Chapter 9: Acknowledgements

First and foremost, I would like to express my sincere gratitude to Professor Saverio Bellusci for his invaluable guidance, support, and encouragement during this study. I am deeply thankful for his role as an inspiring and understanding supervisor and for his kindness and patience. He taught me resilience during difficult times and patiently showed me how to interpret data, construct manuscripts, and develop scientific discussions. His passion, positivity, and energy were a constant source of motivation. I am especially grateful for the friendly and collaborative atmosphere he fostered in the lab.

Special thanks go to Esmeralda Vásquez Pacheco, my peer in the Ph.D. program, with whom I had many insightful discussions on scientific and non-scientific topics. I am also thankful to Dr. Negah Ahmadvand for generously teaching me how to perform pneumonectomy in mice and for sharing valuable experience-based tips. I am also grateful to Dr. Xuran Chu for collaborating with me in Germany and China, and to Leila Sotoode Atefi, a wonderful friend in the lab. Thanks also go to all the members of the Bellusci Lab, whose companionship created a pleasant and encouraging environment that helped ease the daily challenges of experiments. I will always appreciate their support, kindness, and the enjoyable moments we shared.

I would especially like to thank Kerstin Goth for her constant support and kindness. Her help with breeding mice and genotyping was essential to my work. I am also grateful to Beate Harris and Heike Habermann for their administrative assistance and help in translating German documents.

I would also like to express my sincere gratitude to Prof. Soni Savai Pullamsetti, Prof. Ana Pardo-Saganta, Dr. Chanil Valasarajan, and Dr. Anoop Vadakan Cherian for their generous support in providing me with access to their laboratories and equipment. I am also grateful to Prof. Marek Bartkuhn and Dr. Tara Procida for their valuable assistance in analyzing the bioinformatics data.

Finally, I would like to express my heartfelt gratitude and love to my mother, whose encouragement and belief in me have always been a source of strength, and to my brother, whose constant motivation and support have carried me through challenging times. I also wish to honor the memory of my father. I know he would be proud and happy, even though he is no longer with us. May he rest in peace.